PANDA
Precision Measurement of the Proton Asymmetry in Neutron Decay

Ricardo Alarcon, Septimiu Balascuta
Arizona State University

Alexander Komives
dePauw University

Gordon Jones
Hamilton College

Earl Babcock
ILL

Chris Crawford
University of Kentucky

Tim Chupp (Spokesman), Rob Cooper, Archis Joglekar, Monisha Sharma
University of Michigan

Libertad Barron Palos
Universidad Nacional Autonoma de Mexico

Jeff Nico, H. Pieter Mumm, M.Scott Dewey, Tom Gentile, Alan Thompson
NIST

Geoffrey Greene, Hal Lee, Seppo Penttila
ORNL

Vladimir Gudkov
University of South Carolina

Jim Byrne
University of Sussex

Fred Wietfeldt
Tulane University

Stefan Baessler, L.Pete Alonzi, Emil Frlež and Dinko Počanić.
University of Virginia

September 22, 2008

Contents

1 Overview

We propose PANDA@SNS, a measurement of asymmetry of proton emission from polarized neutron beta decay with the SNS Fundamental neutron Physics Beam. The FnPB will provide a unique world class facility and high intensity source of neutrons for a novel suite of experiments. We propose this fundamental experiment because the neutron is the most fundamental unstable elementary particle, because it can be polarized, because there are several more distinct observables than Standard Model parameters, and because we have increasingly more sophisticated tools and techniques: the FnPB, neutron polarization and precision neutron polarimetry, a new spectrometers and new detection techniques. This proposal answers the call to develop experiments that best exploit the FnPB features and greatest advantages, which arise from the time-of-flight dispersion of neutron energy made possible by the pulse structure. The FnPB, will provide precision polarimetry using polarized ^{3}He, discrimination of background and discrimination of neutron wavelength dependent systematic effects, for example spin-flip efficiency and Stern-Gerlach effects.

The goal of PANDA@SNS is a 0.1% measurement, which will require neutron polarimetry, background suppression and control of systematic effects all at the 0.1% level. The proton asymmetry is nearly an order of magnitude larger than the beta asymmetry. Consequently a 0.1% measurement of at FnPB will not be statistics limited, rather we will be able to focus on limiting, measuring and understanding systematic effects and preparing for a subsequent upgraded experiment with the potential to measure well below the 10^{-3} level.

In the context of V/A theory 0.1% measurement of the proton can be interpreted as a 0.15% measurement of λ, the ratio of axial-vector to vector coupling constants with systematic effects much different from those encountered in measurements of the beta-neutrino asymmetry (a) and the beta-spin asymmetry (A). The proton asymmetry is also a sensitive measure of the mechanisms of neutron beta decay and physics beyond the Standard Model and is complementary to other asymmetry measurements.

PANDA@SNS is characterized by the following:

- The FnPB neutron beam will be polarized by either a ^{3}He spin filter or by a polarizing supermirror and the neutron polarization will be measured with a thick ^{3}He analyzer. Tests at LANSCE have demonstrated the feasibility of 0.1% precision in the determination of neutron spin polarization when the time-of-flight dependence of transmission through the ^{3}He is measured.

- A magnetic spectrometer will be instrumented with conventional surface barrier detectors for coincidence detection of the beta and proton from a neutron decay event. Protons will be accelerated through a potential difference of about 25 kV using techniques applied to a number of recent neutron decay experiment, which have also shown that backgrounds can be reduced to below 0.1% for coincidences.

- The proton energy dependence of the asymmetry will be used to study systematic effects to achieve the goal of reducing the combined systematic and statistical error to below 0.1%.

PANDA@SNS is part of a larger program of neutron decay measurements at the FnPB that will use a common magnet facility proposed for this abBA and Nab; however PANDA was originally proposed as an oppotunistic experiment at FnPB that would require more modest resources and conventional technology than abBA/Nab, in particular surface-barrier detectors and a uniform magnetic field. PANDA

is also an outgrowth of the NIST proton-asymmetry experiment, though the approach to neutron polarimetry at NIST would be rather different and in need of further development to reach the 0.1% level.

2 Introduction

The correlation of the recoil proton momentum with the spin of a decaying neutron, arises due to the interference of amplitudes with different transformation properties under parity[1]. The correlation can be expressed as

$$\frac{d^3\Gamma}{dE_p d\Omega_p} = G(E_p)[1 + \kappa(E_p, \Omega_p)C]\hat{\sigma} \cdot \hat{p}_p), \tag{1}$$

where $\hat{\sigma} = \frac{\vec{J}}{J}$, κ is a kinematic factor and C is the parity violating correlation. The coefficient C can be measured in an experiment that extracts the proton asymmetry

$$A_p = \frac{N_+ - N_-}{N_+ + N_-} = kC\mathcal{A}(1 - f)P_n, \tag{2}$$

where N_+ and N_- are, respectively, the number of protons emitted with $\hat{\sigma} \cdot \hat{p}_p > 1$ and $\hat{\sigma} \cdot \hat{p}_p < 1$ integrated over all electron and neutrino energies, P_n is the appropriately averaged neutron polarization *for each neutron spin state*, $\mathcal{A}$ is the analyzing power for proton detection, and f is the fraction of $(N_+ + N_-)$ due to backgrounds. The kinematic factor k depends on the range of the proton energy spectrum that is measured. When integrated over the proton energy spectrum and all solid angles, $k \approx 0.27484$[2]. A 1.5% measurement of kC was reported by the Perkeo collaboration[4] (see Table 1).

For V/A models, in particular the Standard Model, C can be related to $\lambda = |\lambda|e^{i\phi} = g_A/g_V$[1, 3]. Up to corrections of order 0.5%,

$$C = 4\frac{\mathrm{Re}(\lambda)}{1 + 3|\lambda|^2} \approx -0.866. \tag{3}$$

Recoil-order, coulomb, and radiative corrections are discussed in Section 3.2. Non-Standard Model physics, for example arising due to scalar or tensor interactions modify this relation, and thus a set of measurements of neutron decay correlations becomes a probe of new physics.

Unlike the beta asymmetry, which has been the focus of measurements for several decades, precise measurement of the proton asymmetry has been elusive due to the difficulty of measuring the protons, which have a maximum energy of 0.75 keV. Recent work represented by the successes of the emiT experiment[5, 6], the Sussex/NIST/ILL[7] and NIST[8] neutron lifetime experiments, the Sussex/ILL electron-antineutrino correlation experiment[9] and the NIST radiative neutron decay experiment[10], have solved the problem by accelerating the protons to 20-30 keV and detecting them with silicon charged particle detectors. The most important systematic errors for this measurement are from backgrounds, measurement of neutron polarization and imperfect analyzing power of the charged particle spectrometer. Backgrounds have also been mitigated to sufficiently low levels by measuring beta-proton coincidences and can be further reduced by taking advantage of the SNS pulse timing. Neutron polarimetry at the 0.1% level has been shown to be feasible using polarized ^{3}He and time-of-flight discrimination of neutron velocity[11], and a strategy for assessing the spectrometer's imperfections through simulations and measurements is presented here. We show that the expected decay rate for the polarized FnPB beam at 18 meters will be about 1 Hz/cm^3 for a 3.7 Åwavelength bite and a total rate of 35 decays per second is anticipated so that the statistical precision of 0.1% would require fewer than 10 days of continuous data acquisition.

Our ultimate goal is to make the most precise possible measurement of the proton asymmetry to provide reliable input to our knowledge of neutron decay parameters. In particular these results must be combined with the neutron lifetime, which is currently enjoying considerable scrutiny due to the discrepancy of recent results[12, 13]. This measurement must therefore stand alone as an accurate

result that can be used to determine λ in the context of the Standard Model and to probe new physics when compared to other neutron decay correlation coefficients. In this proposal, we have aimed to present an experiment that will be both accurate and provide an impeccable error estimate. Purely theoretically based estimates of experimental corrections must be avoided, and all contributions to the systematic errors must be experimentally corroborated. The proton asymmetry is an independent quantity that can be measured in an experiment with very different systematic limitations compared to other measurements of neutron decay correlations.

PANDA@SNS is part of a superset of neutron beta decay studies being pursued by the US fundamental neutron physics community. The overall goal is complete clarification of parameters of neutron decay. This will require continued work on the neutron lifetime and precision measurements of the decay correlation coefficients (e.g. ACORN, which plans to measure the beta-neutrino correlation, beta asymmetry measurements including UCNA , and the global approach of abBA/Nab). As the neutron lifetime measurement is addressed and resolved, the motivation to make a more precise measurement of λ becomes stronger. Thus a new approach to measuring λ with unique set systematic effects is essential. Our proposed proton decay experiment, PANDA is focused to meet this need. PANDA@SNS, the measurement of C at the 0.1% level at FnPB is a unique opportunity that will provide a crucial measurement with broad impact.

3 Physics Motivation

Since the discovery of the weak interaction, precision measurements in beta decay have been a cornerstone of nuclear physics contributions to developing the Standard Model and to probing new physics. In addition to intrinsic interest in measurement of the parameters of neutron decay, the neutron has been among the most important systems for study of elementary particle physics because the experimental results can be related to the physics of fundamental fermion interactions with the smallest and most reliably calculated corrections. Neutron decay, a four fermion interaction, is described most generally in terms of a set of coupling constants as described below. A full set of measurements is necessary to determine all of the possible coupling constants; however models constrain these by relating the parameters. In the Standard Model, a single parameter, $\lambda = g_A/g_V$ relates A, B,and C as presented in Table 1, thus their direct measurement probes the Standard Model and the possible additional parameters introduced by new physics (*e.g.* scalar interactions). Precision measurement of C provides new input into the global analysis of neutron decay and beta-decay more generally. For example, combining C with V_{ud} determined from super allowed nuclear beta decays[14] provides and indirect measure of the neutron lifetime.

The status of neutron decay is summarized in Figure 1, which shows V_{ud} versus λ from a variety of measurements. Results for two values of the neutron lifetime are shown: the PDG value ($\tau_n = 885.7 \pm 0.8$ s) and the most recent precise measurement ($\tau_n = 878.5 \pm 0.8$ s)[13]. In the Standard Model, the neutron lifetime is given by

$$\tau^{-1} = G_F^2 |V_{ud}|^2 (1 + 3\lambda^2) \frac{m_e^5}{c^5} (1 + \delta_R), \tag{4}$$

where δ_R includes radiative corrections. Figure 1 also separates the PDG and Perkeo-II determination of λ determined from different measurements and shows the precision possible with a 0.1% measurement of C. Also shown in Figure 1 are the results from the most recent analysis of the super-allowed $0^+ \rightarrow 0^+$ decays once a number of corrections are made[14, 15] and the most recent result based on CKM Unitarity and the recently reported measurements of $|V_{us}|$ from a variety of kaon decay experiments.

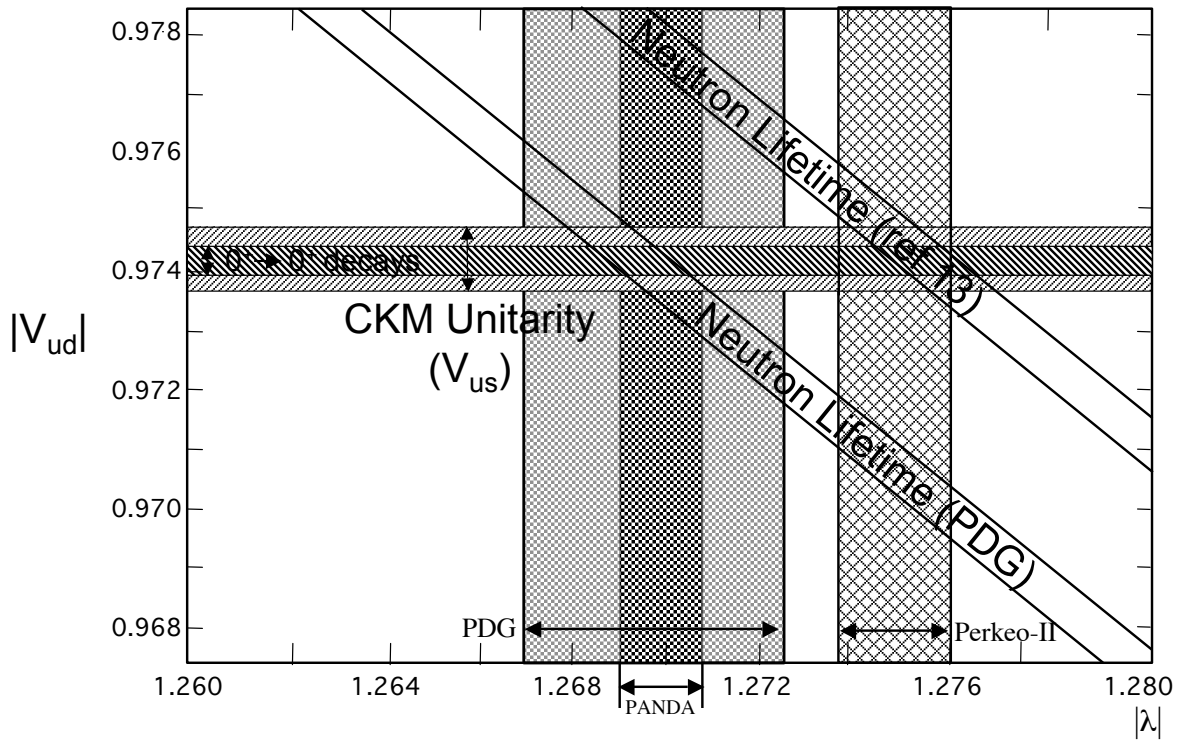

Figure 1: Neutron decay results and V_{ud} from the most recent superallowed decays and from $|V_{us}|$+CKM Unitarity. The band labeled PANDA indicates the role of a 0.1% measurement of the proton asymmetry.

Increased interest in precision measurement of V_{ud} was based o the apparent violation of first-row CKM Unitarity at the 2.5σ level; however the most recent the value of V_{us} leads to remarkable consistency as shown in Figure 1. This consistency does alter the landscape but does not affect the importance of precision determination of V_{ud} in neutron decay. In fact, as the precision of V_{ud} from super-allowed decays improves, the neutron results must also improve in order to more precisely probe the Standard Model and Physics Beyond. As shown in Figure 1, the current uncertainty in V_{ud} from neutron decay is dominated by the uncertainty in λ. The goal of PANDA is to reduce this uncertainty.

It is important to note that λ is a parameter in the context of the Standard Model or more general Vector/Axial Vector models *i.e.* $\lambda = g_A/g_V$, i.e models that include right-handed currents. Comparing values of λ extracted from measurements of two or more neutron beta-decay correlation coefficients from the forms given in Table 1 with appropriate corrections thus becomes a test of the Standard Model: if the value of λ is not consistent the explanation must include new physics. By the same token, using λ and the neutron lifetime to determine $|V_{ud}|$ is based on the Standard Model. A discrepant value of $|V_{ud}|$ derived in this way is a signal of new physics. The possibility of a right-handed boson with different couplings and greater mass than the Standard Model W would modify the correlation coefficients, for example B, which is nearly unity in the Standard Model because the antineutrino is right handed. Right handed currents introduce additional parameters in a Vector/Axial Vector theory. The results of a variety of experiments combine to restrict the possible values of the mass and mixing angle of a right-handed W. The proton asymmetry coefficient C is sensitive to right-handed currents, and a 0.1% measurement combined with an independent measurement of A would significantly improve the current limits. Non Vector/Axial Vector interactions, for example scalar leptoquarks, which transform a quark into a lepton have also been proposed and investigated[16].

Neutron decay also is crucial to the rapidly evolving field of precision cosmology through Big

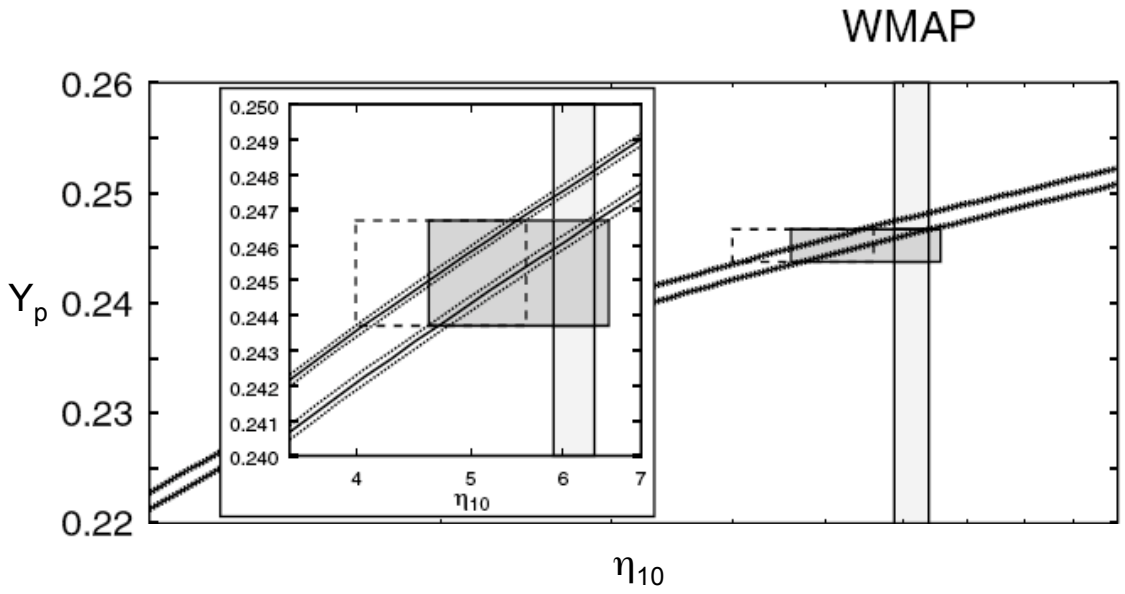

Figure 2: The primordial ^{4}He abundance as a function of the baryon-to-proton ratio $\eta_{10} = 10^{10}\eta$. The inset shows an expanded view near the allowed region. The upper band is based on the PDG recommended neutron lifetime and the lower band is based on reference 13.

Bang Nucleosynthesis (BBN). The neutron lifetime and V_{ud} bear directly on the determination of the baryon-to-photon ratio, the baryon asymmetry η. For example, a larger value of V_{ud} implies that the limiting weak interaction rates remain greater than the constant expansion rate longer resulting in a lower neutron-proton ratio (n/p) at freeze out. Similarly, a shorter neutron lifetime reduces n/p. The observable consequence in the current universe is the ^{4}He abundance, Y_p, which also depends on η as shown in Figure 2, which is from reference [17]. The role of PANDA and λ in would come through either the determination of V_{ud} or the indirect determination of τ_n using λ and V_{ud} from super allowed beta decays; however to avoid circular reasoning, it is probably better to take a global approach using all measurements to adjust the BBN model input parameters.

The determination of λ bears directly on the rate of themonuculear reactions in the sun. The process $p + p \rightarrow {}^2\mathrm{H} + e^+ + \nu_e$, is inverse neutron decay; however the protons combine in the singlet state while the deuteron is spin 1. Thus the process is pure Gamow-Teller with rate proportional to $g_A^2 = |V_{ud}|^2\lambda^2$. The Borexino Collaboration has very recently reported observation of neutrinos from the pep branch. Though the the uncertainty in g_A does not practically impact the interpretation of the neutrino results, solar models are extremely precise and require high precision on the input parameters.

3.1 General Formulation of Neutron Decay

The interaction Hamiltonian for beta decay, assuming only Lorentz invariance and separate currents of hadrons and leptons can be written

$$\mathcal{H} = \sum_i (\bar{p}\Gamma_i n)(\bar{e}\Gamma_i(C_i + \gamma_5 C_i')\nu) + \mathrm{H.C.}, \tag{5}$$

where the Γ's are complex operators made up of combinations of the Dirac gamma-matrices, the subscript i spans the five fermion operators allowed by Lorentz-Invariance,i.e. $i = S, P, V, A, T$ (Scalar, Pseudoscalar,Vector, Axial-vector, and Tensor). In the Standard Model, only V and A are allowed, and

due to CVC, there is only one form factor so that a single parameter (λ) connects the quark interaction to neutron decay. The weak interaction can also mix the generations of quark flavors, *i.e.* u-d, c-s, and t-b. This mixing is described by a unitary matrix V_{ij} (the CKM matrix). In neutron decay a d-quark transforms into a u-quark as a vector or axial vector current with an amplitude proportional to V_{ud}. In principle, the C_i's are determined by experiment, and are tightly constrained [18] with

$$C'_V/C_V \approx 1 \qquad\qquad C'_A/C_A \approx 1 \qquad\qquad C^{(\prime)}_{S,T} \approx 0.$$

These are consistent with the Standard Model in which only vector and axial vector currents mediate the weak interactions, and only left handed projections of the quark spinors are isodoublets, while the right-handed projections appear as isosinglets. Other terms leading to scalar currents and right-handed couplings are not present in the Standard Model, but would appear in a more general formulation. New physics, i.e. beyond Standard Model Physics, could appear in the form of Right-handed currents, *i.e.* beta-decay mediated by a heavy W-boson that couples to right-handed isodoublets or scalar interactions. Leptoquarks, which mediate scalar couplings of quark to a lepton, *e.g.* $\bar{\nu} \rightarrow u$ and $d \rightarrow e$, carry fractional charge, lepton number and baryon number.

3.2 Polarized Neutron Decay

The most general formulation of the decay rate for neutrons polarized along $\vec{J}$ with no polarization analysis in the final state was written down by Jackson, Treiman and Wyld[19]:

$$\frac{d\Gamma}{dE_e d\Omega_e d\Omega_\nu} = \frac{1}{\tau_n} G(E_e)\{1 + a\frac{\vec{p}_e \cdot \vec{p}_\nu}{E_e E_\nu} + b\frac{m_e}{E_e} + \hat{\sigma}_n \cdot (A\frac{\vec{p}_e}{E_e} + B\frac{\vec{p}_\nu}{E_\nu} + D\frac{\vec{p}_e \times \vec{p}_\nu}{E_e E_\nu})\}. \tag{6}$$

The coefficient b is zero in the Standard Model, but would be non-zero if scalar interactions, such as extra Higgs boson or lepto-quark exchange, exist and $C_S^{(\prime)} \neq 0$. The coefficient D has contributions at the 2×10^{-5} level from final-state effects and from an imaginary part of λ, which would require time-reversal violation. The coefficients a, A, and B depend on λ as discussed below. Equation 6) is written in terms of neutrino momentum. Though the neutrinos are not directly observed, this form is useful because it covers the entire kinematically allowed phase-space. The angular correlation coefficients and Standard Model formulae to lowest order are given in Table 1. At tree level, we have

$$C = -(A + B). \tag{7}$$

The coefficients a, A, B, etc. depend on the momenta due to radiative and higher order corrections which are of order 10^-3, the sensitivity goal of PANDA@SNS. For example[20, 22],

$$B \rightarrow \tilde{B}(E_e)$$

$$A \rightarrow \tilde{A}(E_e) + \tilde{A}'(E_e)\frac{\vec{p}_e \cdot \vec{p}_\nu}{E_e E_\nu}. \tag{8}$$

Thus precise energy calibration for both proton and electron is useful to separate Standard Model radiative corrections from new physics. For the proton asymmetry, C, extracting specific physics, e.g. g_A from C requires that thesef radiative and recoil-order corrections be taken into account. For the proton asymmetry, these corrections have been calculated by Gluck[3], and additional assessment by Gudkov and collaborators is underway[23]. The importance of these corrections in the analysis is discussed further in section 4.11.

Table 1: Values and tree-level Standard Model formulae for neutron beta decay correlation coefficients.

λ	-1.2695 ± 0.0029[12]	SM (lowest order)	$\lvert d\lambda/dx \rvert$	$\lvert \frac{\sigma_\lambda}{\lambda} \rvert / \lvert \frac{\sigma_x}{x} \rvert$
a	-0.103 ± 0.004 [12]	$\frac{1-\lvert\lambda\rvert^2}{1+3\lvert\lambda\rvert^2}$	3.227	0.2618
A	-0.1173 ± 0.0013 [12]	$-2\frac{\mathrm{Re}(\lambda)+\lvert\lambda\rvert^2}{1+3\lvert\lambda\rvert^2}$	2.661	0.2459
B	$+0.983 \pm 0.004$ [12]	$-2\frac{\mathrm{Re}(\lambda)-\lvert\lambda\rvert^2}{1+3\lvert\lambda\rvert^2}$	13.66	10.58
C	-0.865 ± 0.013[4]†	$4\frac{\mathrm{Re}(\lambda)}{1+3\lvert\lambda\rvert^2}$	2.193	1.494
D	-0.0004 ± 0.0006 [12]	$\frac{\mathrm{Im}(\lambda)}{1+3\lvert\lambda\rvert^2}$		
ϕ	180.06 ± 0.0029 [12]			

† The authors report $kC = -0.2377 \pm 0.0036$.

The sensitivity to λ of a proton asymmetry measurement compared to that of other correlation coefficient measurements is shown in the last column of Table 1. The sensitivity to λ of C appears somewhat less than that of A or a, however note that the proton asymmetry is nearly an order of magnitude larger than the beta asymmetry, and thus the measurement is subject to different and arguably less complicated systematic errors. For example electron backscattering are dominant in a measurement of A and precision proton energy spectroscopy required to determine a and B. (The aCorn experiment has cast measurement of a into an asymmetry measurement). A measurement of C with uncertainty 0.1% and accurately calculated corrections (for a 0.1% measurement of C, the Coulomb corrections to C must be calculated to about 10%) will have significant impact on determining λ and thus g_A and, when combined with the neutron lifetime and G_F, on V_{ud}. Moreover, C is a measure of the amount of parity violation in neutron decay, and is thus also sensitive to non-VA couplings when combined with other correlation coefficient measurements, i.e. consistency of λ from independent measurements of A and C is a prediction of models with only vector and axial vector couplings.

In Figures 3 and 4 we show the proton asymmetry C as a function of proton energy for varying values of λ, and B assuming tree level physics (i.e. energy independent couplings). In Figure 3, the Standard Model relations given in Table 1 are used with three values of λ. In Figure 4, only B is varied, with A fixed, thus indicating physics beyond the Standard Model. A more complete study including radiative corrections is underway, however the utility of proton (and beta) energy resolution is clearly illustrated. As discussed in section 5, proton and electron energy resolution also provide crucial systematic checks.

3.3 Summary of Motivations

Measurement of the proton asymmetry is an essential component of the role of neutron decay in nucleosynthesis, the solar energy cycle, determination of V_{ud}, and the search for new physics beyond the Standard Model. The FnPB will provide high neutron fluxes sufficient for statistically precise measurements and the essential feature of time-of-flight combined with polarized ^{3}He for precision neutron polarimetry. The PANDA experiment will provide redundant measures of analyzing power and background effects not possible in the reactor based experiments. The possible additional neutron spin flip provided if a ^{3}He spin filter is used add additional systematic checks. PANDA is a unique new experiment that answers the call to exploit the unique features of the FnPB for fundamental neutron physics.

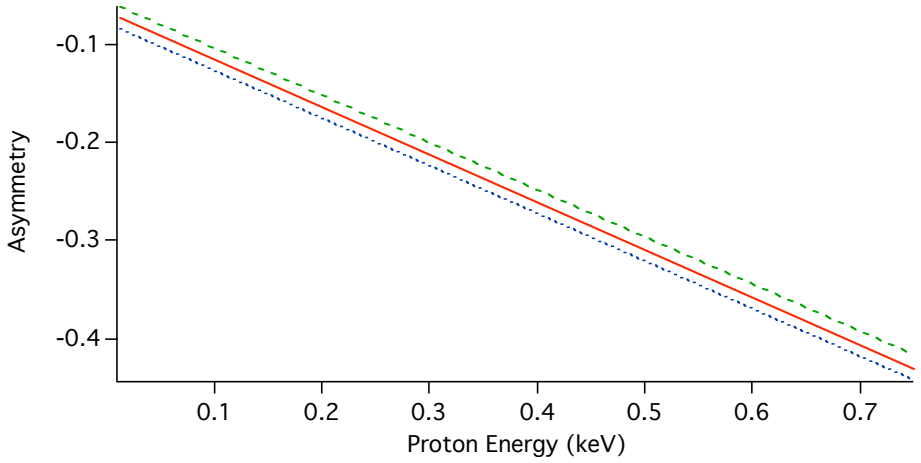

Figure 3: The proton asymmetry kC as a function of proton Energy for $\lambda = -1.1$ (dotted line), $\lambda = -1.2$ (solid line) and $\lambda = -1.3$ (dashed line)

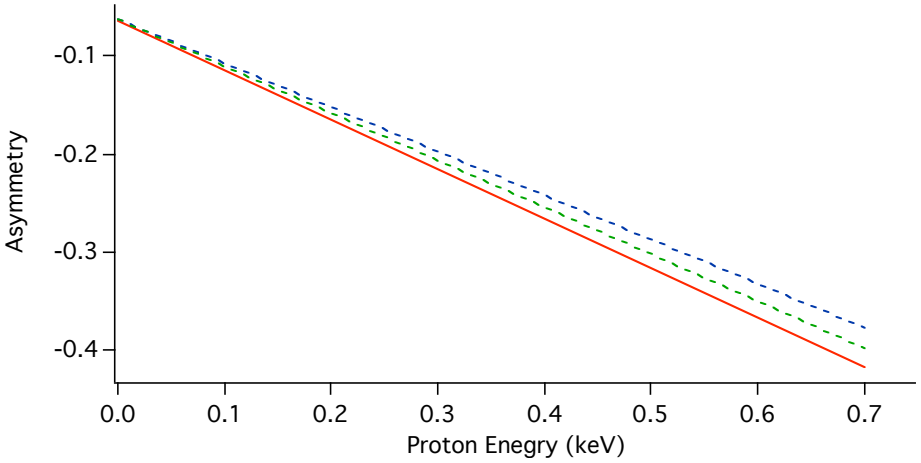

Figure 4: The proton asymmetry kC as a function of proton Energy for $B = 0.90$ (dashed line), $B = 0.95$ (dotted line) and the PDG value $B = 0.9851$ (solid line)

4 Experimental Details

PANDA has the following requirements:

- A high intensity polarized neutron beam that transports the polarized neutrons through the experiment and flips the neutron spin with respect to the guide field.
- High precision measurement of neutron polarization and spin flip efficiency
- A spectrometer that detects beta-proton coincidences with high efficiency
- Near perfect proton analyzing power (identification of the direction of the protons with respect to the spectrometer axis)
- Proton energy measurement
- Low backgrounds
- Complete Monte Carlo modeling of the experiment including tracking, scattering and backscattering and detector responses
- Direct determination of systematic effects including efficiencies, charged particle scattering and backscattering, and analyzing power
- A defined upgrade path

4.1 Measurement Principle

The proposed layout is shown in Figure 5. The neutron beam is collimated and passes through a polarizer, either polarized ^{3}He or a crossed supermirror, a spin flipper, and the spectrometer. A thick ^{3}He polarization analyzer followed by thick neutron detector is placed downstream of the detector. The entire experiment must be held in a magnetic field that transports the neutron spins adiabatically from the polarizer to the analyzer through the detector field, and is tailored to the requirements of each element of the experiment.

Polarized neutrons enter the detector fiducial volume polarized along or opposite the magnetic field $\vec{B}$. Consider a neutron decay with the proton emitted parallel to $\vec{B}$: it will drift and spiral along the $\vec{B}$. An electric field generated by the potentials sown in Figure 6 will accelerate the proton to about 24 kV and onto a silicon detector, most likely a silicon surface barrier detector (SBD). If the neutron spin is transported adiabatically, *i.e.* $\hat{\sigma}_n$ IS parallel to $\vec{B}$, the analyzing power $\mathcal{A}$ will differ from unity only due to proton scattering/backscattering and imperfections in the magnetic field profile, i.e. the bottle effect and the electric fields. Backgrounds will be reduced by requiring coincidence with an electron detected with 4π solid angle (*i.e.* no directional information for electron detection). A coincidence measurement will, introduce an electron energy threshold of of 24 keV, which may affect the relation in equation (3); however only 0.15% of the electron spectrum lies below 24 keV and the correction is small. Proton energy resolution is provided by a depression of the potential V_0 in the decay region by up to 1 kV. With the potential set to V_0, only protons with longitudinal momentum satisfying $p_z > \sqrt{2em_pV_0}$ reach the detector.

The crux of a 0.1% measurement requires sufficient count rates and precise knowledge of backgrounds, solid angles for detection of protons, and the neutron polarization. All must be measured to much better than 0.1%. In the following, we argue that a measurement with this precision and better is feasible, and that the FnPB is ideally suited for these measurements.

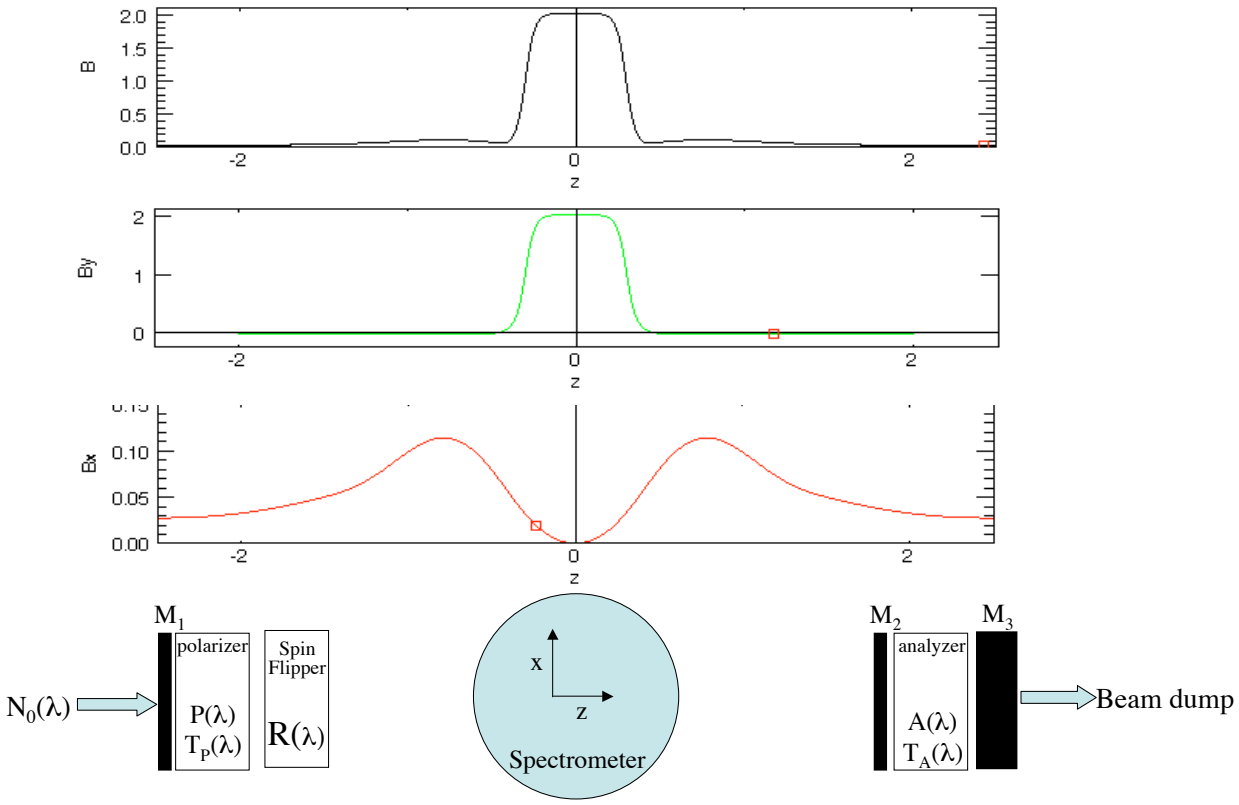

Figure 5: The general layout of a proton asymmetry measurement of flight path 13. The magnetic field in the spectrometer is directed along $\hat{y}$, into the page; the field B_x is the neutron guide field to and beyond the spectrometer. The total magnetic field, shown at the top, does not pass through zero to ensure adiabatic transport of the neutron spin. The polarizer and analyzer are in uniform regions of the guide field, and the AFP-spin flipper is in a region of magnetic field gradient. The individual elements of the experiment are discussed in separate sections.

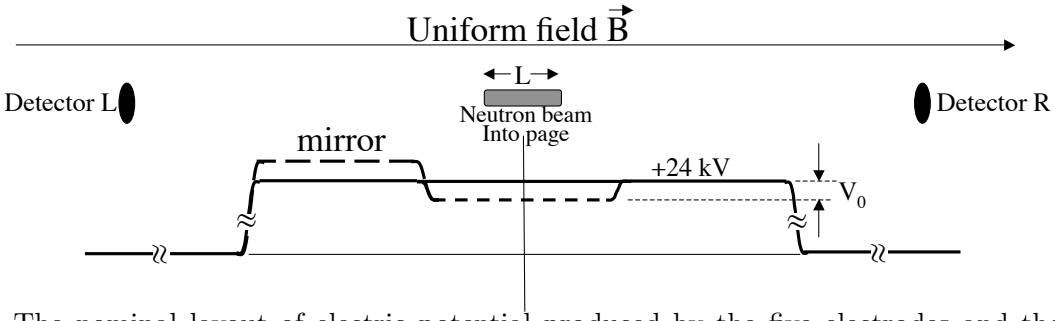

Figure 6: The nominal layout of electric potential produced by the five electrodes and the uniform magnetic fields for the PANDA spectrometer. The potential depressed by V_0 in the fiducial volume is used in the proton energy analysis mode. The proton mirror configuration can be set at either side to study the spectrometer analyzing power.

4.1.1 Coincidence Measurement

The proton asymmetry as defined in equation 2 implies a proton singles measurement; however PANDA is designed to be a coincidence measurement to reduce background. Ideally all betas would be detected with no angular dependence to the detection efficiency, and thus the coincidence just serves to ensure that the 24 keV proton in the SBD was from a neutron decay. The caveats arise due to energy and position/angular dependence of the beta detectors. Weinberg has shown that if the electron (and neutrino) momentum and spin is NOT measured, i.e. the entire electron spectrum is integrated, then equation 3 is valid for any V/A theory[24]. The problem is that electrons with energy less than 24 keV will be trapped at the center of the spectrometer and thus beta energy is in some sense "measured." In Figure 7 we show that for these low beta energies, the effect on the proton asymmetry is small and calculable.

4.1.2 Proton Energy Dependence

Very low energy protons will drift so slowly from the spectrometer decay region before being accelerated to 24 keV by the electric field that they will time out of the beta-proton coincidence window. Figures 3 and 4 show the variation of the asymmetry as a function of proton energy. The retarding potential V_0 will allow measurement of the integrated proton asymmetry above the threshold and will be used to calibrate the proton energy. Precise modeling of the experiment will include this effect.

4.2 The FnPB Beam

The FnPB beam will emerge from a 10 cm wide by 12 cm tall neutron guide. We assume the PANDA apparatus will be oriented with a magnetic field in the vertical direction with an acceptance of 3-4 cm wide by 10 cm tall. The pulsed beam introduces a time-of-flight dependent density of polarized neutrons in the spectrometer decay region given by

$$\rho_n(t) = \int \frac{d\phi(\lambda, \vec{r})}{d\lambda} \, \frac{1}{v} \, d\lambda, \tag{9}$$

where, $\phi(\lambda, \vec{r})$ is the neutron flux density and, for a distance $L =$ m from the moderator,

$$t = \frac{L}{v} \qquad \text{and} \qquad \frac{1}{v} = \frac{m_n \lambda}{h}. \tag{10}$$

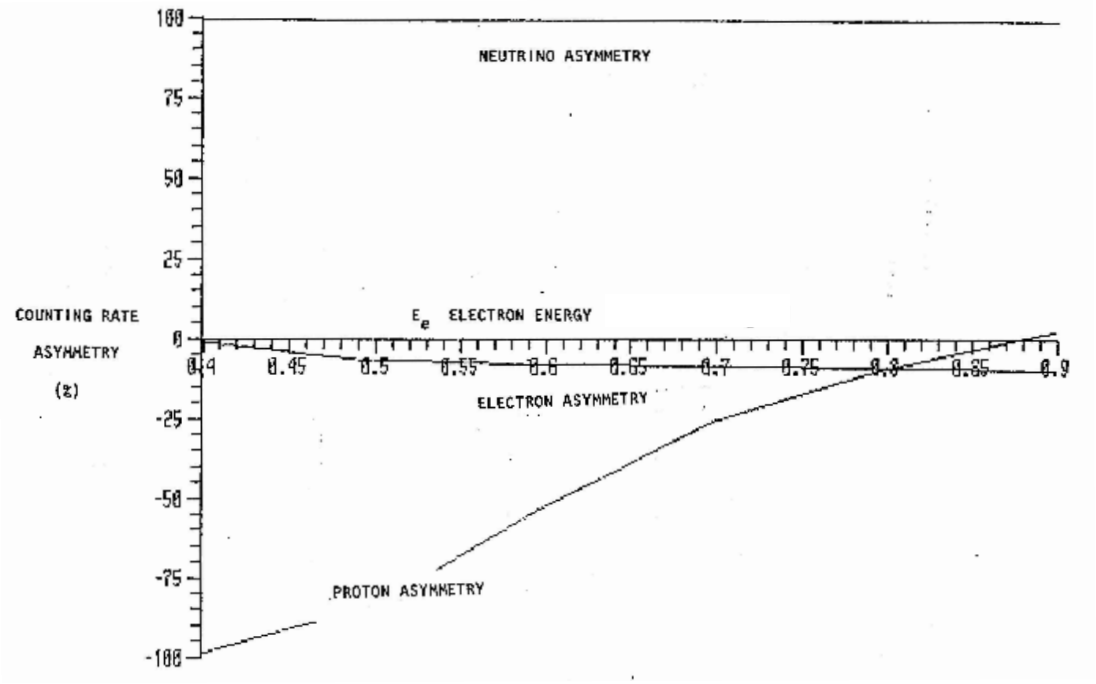

Figure 7: The neutrino, beta and proton asymmetries as a function of beta energy expressed as a percentage of kC. Electron energies are expressed in units of the maximum energy E_{max}. For beta energies below 0.4 E_{max}, the contribution to the proton asymmetry is quite small. Graph from J. Byrne, A Proposal to Measure the Angular and Polarization Correlation Coefficients in Neutron Decay.

The performance of the FnPB has been studied through simulations of the SNS spallation source and FnPB beam line, and the estimates presented here are based on these simulations. [25]. Optimization of the cold beamline includes characterization of the guides and benders, the neutron transmission through the 0.89 nm monochromator installed for the UCN beam line, and the expected performance of time-of-flight chopper. Projections are for flight path 13, assuming the initial projected SNS power of 1.4 MW and a super mirror guide with $m = 3.6$. The numerically simulated spectrum is well approximated by

$$\frac{d\phi}{d\lambda} = e^{-(\lambda_0/\lambda)^\gamma} \frac{A}{\lambda_0} (\frac{\lambda_0}{\lambda})^\beta, \tag{11}$$

with $\lambda_0 = 3;\ \beta = 1.6;\ \gamma = 3.4;$ and $A = 2 \times 10^9$ n/cm^2/s.

The flux of polarized neutrons depends on the polarizer. For ^{3}He, the transmission and polarization depend on λ as described below, while for a crossed super mirror, the transmission and polarization are quite uniform in the range of $2 \leq \lambda \leq 10$ Å. In Figure 8, we show the estimated flux of polarized neutrons and the neutron density as a function of wavelength for each polarizer assuming an optimized spin filter with 60% ^{3}He polarization and crossed supermirrors (XSM) with a total transmission of 0.12. The average neutron decay rate per unit volume and wavelength is $\mathcal{R}(t) = \rho_n(t)/\tau_n$. The wavelength dependence of the neutrons in the decay region of the spectrometer for both polarizers is shown in figure 9. The density is porportional to $1/v$, i.e. proportional to the time a neutron spends in the decay region.

Choppers are employed to avoid frame overlap. For 60-Hz operation, a wavelength bite of $\Delta\lambda = 3.7$ Å can be used at 18 m. As discussed in section 5, possible systematic errors include neutron spin dependent and neutron spin independent interactions. The super mirror polarizer and the ^{3}He neutron spin filter introduce different wavelength or time-of-flight dependences. In general, the choice of wavelength bite should maximize the figure of merit ($P_n^2 T_n$); however it is useful to use a different wavelength bites for systematic error studies. The set of frame overlap choppers can be tuned, for example to increase the flux of faster neutrons. The total neutron decay rate per unit volume for a wavelength bite chosen to maximize the figure of merit is given in Table 2 for each polarizer and for three different ^{3}He polarizations with the optimized figure figure-of-merit (FOM) and for 90% average neutron polarization. The average polarization is given by

$$< P_n >= \sqrt{\frac{\int P_n(\lambda)^2 \frac{d\phi(\lambda,\vec{r})}{d\lambda}\ \frac{1}{v}\ d\lambda}{\int \frac{d\phi(\lambda,\vec{r})}{d\lambda}\ \frac{1}{v}\ d\lambda}}. \tag{12}$$

As the ^{3}He polarization changes, a different combination of P_n and transmission optimized the figure of merit.

4.2.1 Beam Line Monitors and Neutron Detectors

Two thin and one thick monitor will be used to monitor the neutron beam and for the neutron polarimeter as shown in Figure 5. The detectors similar to the ^{3}He proportional counters used at LANSCE[11] will be sufficient. The neutron polarimeter or a second polarimeter can also be temporarily placed upstream of the spectrometer for studies of neutron spin transport; however this will be in a magnetic field gradient, and the feasibility needs further study.

Table 2: Total polarized neutron decay rates for an optimized 3.7 Å momentum bite. In order to emphasize the trade-offs for the ^{3}He polarizer with 50%-70% polarization, we present the optimized FOM parameters as well as parameters that will provide $\geq 90\%$ average neutron polarization. The FOM is normalized to the crossed supermirror.

Polarizer	Wavelength Bite (Å)	$d\mathcal{R}/dV$ (s^{-1}/cm^3)	$< P_n >$	FOM
^{3}He spin filter (50%)	2.8-6.5	1.9	70%	0.94
^{3}He spin filter (60%)	2.8-6.5	2.1	78%	1.28
^{3}He spin filter (70%)	2.8-6.5	2.5	84%	1.77
^{3}He spin filter (50%)	2.3-6.0	0.8	90%	0.65
^{3}He spin filter (60%)	2.4-6.1	1.4	90%	1.14
^{3}He spin filter (70%)	2.6-6.3	2.1	90%	1.71
Supermirror [26]	2.8-6.5	1.0	99.7%	1

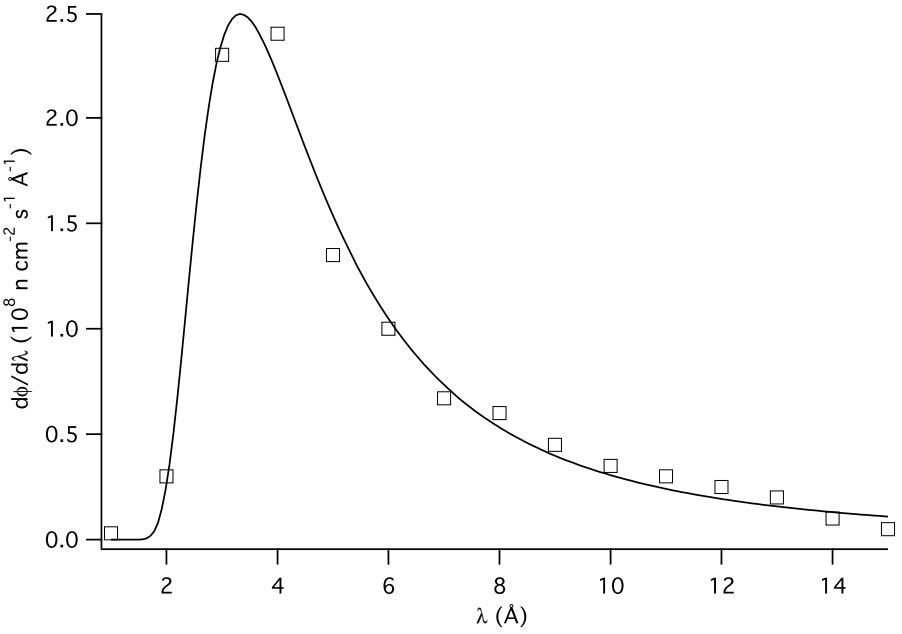

Figure 8: Predicted FnPB flux vs. neutron wavelength for 1.4 MW. The solid line is the model based on equation 7 and the squares are the results of the studies described by Huffman et al. in reference [25]

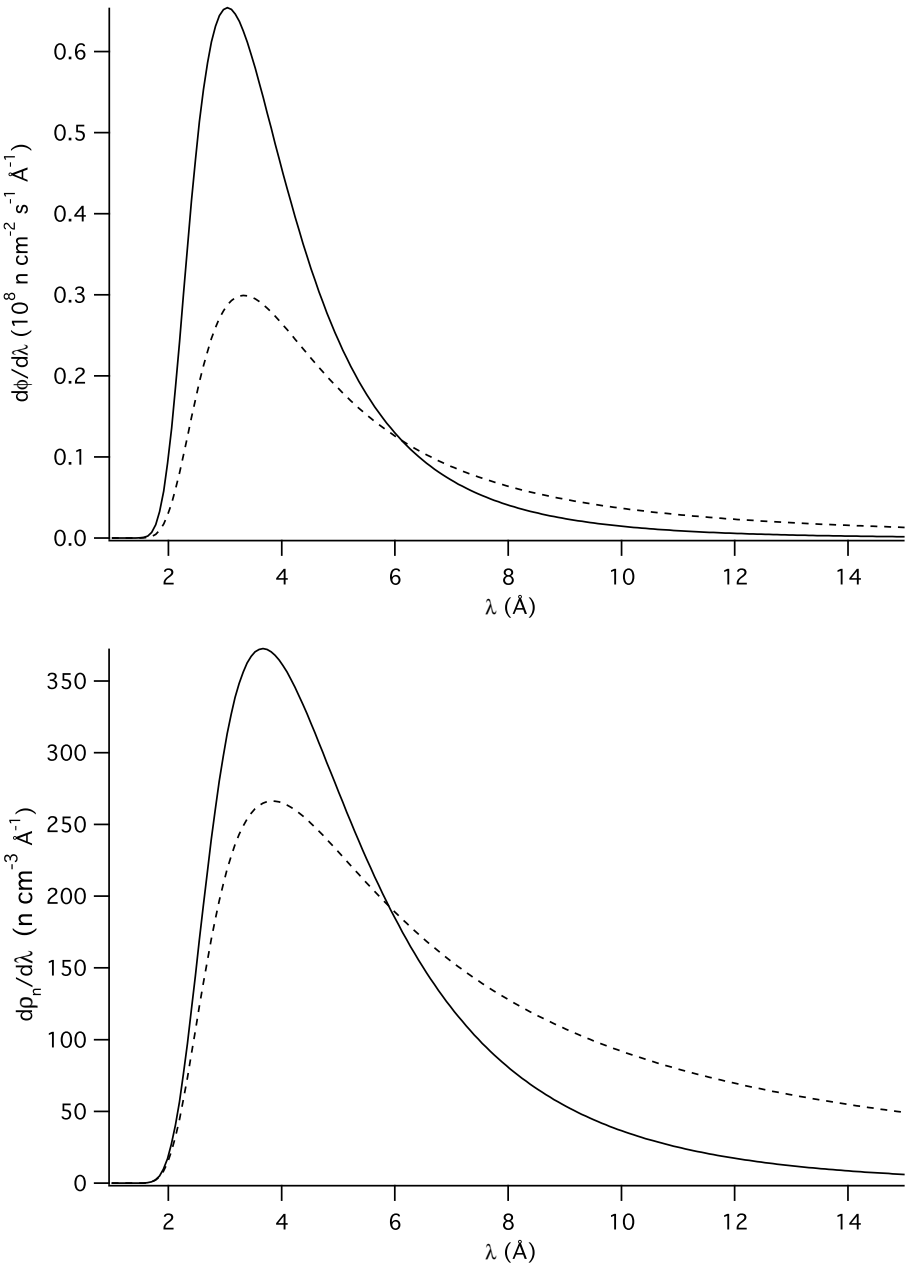

Figure 9: Polarized neutron flux density (top) and neutron density (bottom) as a function of wavelength for the 60% polarization^{3}He spin filter (solid line) and crossed supermirror (dashed line) polarizers.

4.2.2 Cave and Shielding Requirements

The cave will be designed so that it meets the experimental requirements and at same time is an integral part of the radiological and magnetic shielding. Radiological shielding of the PANDA experiment has to be according to the SNS shielding requirements. Design of the shielding will be modeled considering different operation modes of the experiment. The specific feature of the PANDA is the polarizer that will be a significant scattering source on the upstream end of the experiment and will most probably require its owns shielding structure.

The PANDA experiment must also meet the Facility's requirement for stray magnetic fields, i.e. that at the boundaries of the neighboring beamlines stray fields should be less than 50 mG. The spectrometer magnet and the magnetic shielding of the FNPB will be designed so that this requirement is met. Shielding of the SBD detectors will be integrated into the overall cave shielding design.

4.2.3 Beam Dump

The beam dump must be designed to minimize background as well as to meet the facility radiation containment requirements.

4.3 Polarization

There are two possible ways to polarize the beam: a polarized ^{3}He spin filter and a crossed supermirror polarizer. As shown in Table 2, the expected decay rates for an optimum 3.7 Å momentum bite are greater for the ^{3}He spin filter if 60% polarization is maintained, but the intensity averaged polarization is lower for the ^{3}He. The standard figure of merit, $FOM = P_n^2\mathcal{R}$, which is proportional to the inverse of the running time for a fixed statistical error, is 10-20% greater for ^{3}He at 60% polarization. Thus the choice of polarizer depends on cost, reliability, projected and demonstarted improvements (to the ^{3}He) and most importantly systematic effects and systematic checks afforded by the choice of polarizer. In the sections below, we present a discussion the current state of the art of the two polarizers. We conclude that once the ^{3}He polarization issues are solved it is a better choice. The ^{3}He spin filter provides an additional neutron spin flip becasue the ^{3}He polarization can be reversed with adiabatic passage NMR with negligible loss of polarization. In addition, the ^{3}He provides a predicable variation of neutron polarization as a function of time of flight and thus a potentially useful additional systematic check. The ^{3}He spin filter also allows us a more straightforward way to make unpolarized measurements because removing the ^{3}He cell does not change the beam trajectory. The XSM is a fixed device that would be very well characterized by use of a polarized ^{3}He polarimeter, but, as noted, does not allow the additional spin flip and independent method of characterization of the spin flipper. The cost of a pair of 12 cm $\times$ 12 cm supermirror polarizers is on the order of \$150K, comparable to the long-term cost of a well engineered ^{3}He polarizer; however the investment in ^{3}He is essential for the polarimeter, thus there is some possible economy of scale.

4.3.1 Supermirror Polarizers

The crossed supermirror polarizer was developed at ILL[26] to address shortcomings of the single supermirror polarizer, i.e. unacceptable variation of neutron polarization across the beam phase space (position and angles) and as a function of neutron wavelength. The XSM provides very high neutron polarization across a broad wavelength range: 99.7% was measured with an opaque ^{3}He analyzer over the range from 3-7 Å with errors less than 0.1%, as shown in Figure 11 [26]. Unlike the conventional

supermirror, the polarization is also flat (to about 0.1%) over an angular range of -6 to 10 mrad. The absolute transmission is stated to be 50% of that for a single supermirror, but depends on the details of the collimation and beam line. In particular matching of the phase space of the FnPB with $m = 3.6$ to the super mirror with, e.g. $m = 2.8$. An XSM transmission of 0.12 is expected[27]. Note also that development of the beam line with an XSM requires empirical optimization, i.e. measurement of "rocking curves." We are working with the ILL to design and develop cost estimates for a pair of pair of 12 cm $\times$ 12 cm supermirror polarizers.

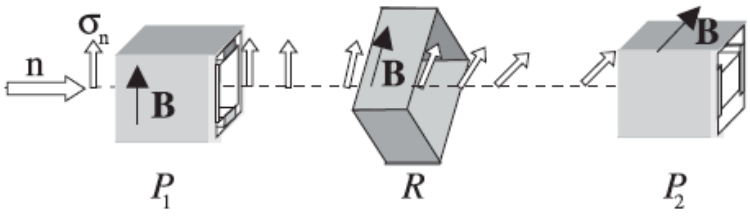

Figure 10: Set-up of crossed supermirrors used at ILL.

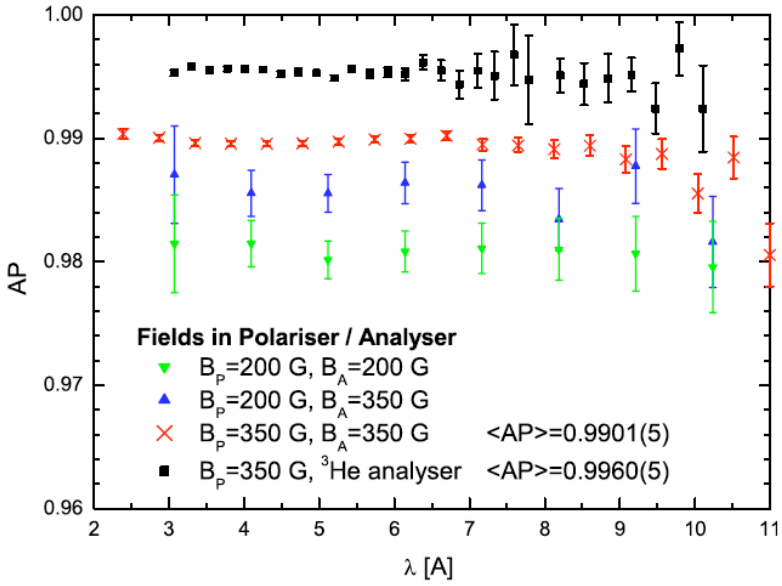

Figure 11: Measured polarization product for the XSM from reference[26]. The ^{3}He method is similar to the polarimetry technique that will be used for PANDA.

4.3.2 ^{3}He Spin Filter

Polarized ^{3}He may be used for the neutron polarizer and will be used for the neutron polarimeter, as discussed below. Polarized ^{3}He[28, 29, 30, 41], has become a widely used technology applied to polarized electron scattering and polarized neutron experiments [31, 32, 33] as well as neutron scattering [34] and lung imaging[35, 36]. Twenty years of applications have led to increasing demands on volume, uniformity, long term stability, diagnostics and magnitude of the ^{3}He polarization. with the most demanding application ddeveloped for the $n + p \rightarrow d + \gamma$ experiment, which ran up to Fall 2006 at Los Alamos.

The basis of the spin filter is the spin dependence of the absorption cross section for neutrons on ^{3}He. The large absorption cross section, $\sigma_a = \sigma_0 \frac{\lambda}{\lambda_0}$, where $\sigma_0 = 5333$ b, is due to an unbound 0^+ resonance in ^{3}He+n [37], thus absorption is possible only only for neutrons with spin opposite to the ^{3}He spin (singlet state). Since the ^{3}He polarization in a polarizer is not perfect, neutrons of both spin states are absorbed, though with different absorption lengths. Thus the transmission and polarization of the neutrons are wavelength dependent:

$$P_n = \tanh(P_3 \sigma_0 t_3 \frac{\lambda}{\lambda_0}) \qquad T_n = e^{-\sigma_0 t_3 \frac{\lambda}{\lambda_0}} \cosh(P_3 \sigma_a t_3 \frac{\lambda}{\lambda_0}), \tag{13}$$

Here P_3 is the ^{3}He polarization, and t_3 is the ^{3}He thickness (atoms/cm^2). The unbound ^{4}He resonance decays to a proton and triton with 782 keV total energy, and no gamma. Possible effects of the ionization are described below.

Two techniques for ^{3}He polarization are used in practice: metastability exchange and spin exchange with laser polarized alkalis and alkali mixtures. For spin filter polarizers that are expected to run with stable polarization for many weeks the spin-exhange technique is most practical, because the metastability-exchange technique polarizes the ^{3}He off-line, and the polarization decays slowly with time constants typically several days.

For the $n+p \rightarrow d+\gamma$ experiment, cells blown from GE180 glass[38] were filled to about 1 atmosphere pressure (at room temperature) with ^{3}He and a small amount of N_2, required for optical pumping[28]. The N_2 also affects recombination of ions and electrons. The role of N_2 in ion recombination is being revisited due to neutron beam effects on the Rb and ^{3}He polarization that are discussed below. The GE-180 glass is boron-free-alumino-silicate glass, with much less neutron absorption than normal boro-silicate glass. Of the seven cells selected as candidate cells for the $n + p \rightarrow d + \gamma$ experiment, three have been used extensively in the neutron beam of long periods. Measurements at NIST with narrowed lasers produced 70%-75% polarization in the cells originally made for $n + p \rightarrow d + \gamma$, but in use at Los Alamos, the maximum polarization was about 55% consistent with what was measured at NIST with broad-band lasers. Narrowed lasers will definitely be used in the next generation of ^{3}He spin filters.

During $n + p \rightarrow d + \gamma$ development runs, we observed neutron beam effects on the ^{3}He polarization that have been further studied in a dedicated run at LANSCE during summer 2007. The summer 2007 run demonstrated that the primary effect is a reduction of the polarization of laser optically pumped rubidium. We are taking part in further studies at high intensity in November 2007 at ILL. The ^{3}He polarization for the cell used over two months from fall 2006 is shown in Figure 12. Though the ^{3}He polarization appears relatively constant (except for the period with the laser off), there is evidence of a slow downward drift. The long time constant appears to be due to reduced laser light transmission through the cell associated with a milky-white appearance that builds up over time in the cells. This build-up is probably due to rubidium chemistry (i.e. formation of Rb-X molecules), either due to the very long periods that the cells have been hot for the $n + p \rightarrow d + \gamma$ experiment or possibly

due to reaction with the hydrogen (protons and tritons) produced by neutron absorption. For the $n + p \rightarrow d + \gamma$ experiment, about 10^{15} hydrogens are produced per month, and several micrograms of RbH would be produced. Examination on shorter time scales (bottom panel of Figure 12) reveals that there are significant drops in the polarization whenever the neutron beam is turned on, and with the beam off, the polarization recovers, at least partially, with the spin exchange time constant. With the beam on, the polarization decays with a time constant on the order of 12 hours (for the Pebbles data) and with the beam off, the polarization recovers. Though the recovery time constant is not measured because we use the neutron beam to measure P_3, it is likely to also be on the order of 12 hours. (The time constant can be measured with NMR.) This time constant is quite similar to the spin-exchange time constant. The time dependence of ^{3}He polarization, with initial polarization $P_3(0)$ is given by

$$P_3(t) = P_3(0) - [P_3(\infty) - P_3(0)][1 - e^{-t(\gamma_{SE}+\Gamma)}], \tag{14}$$

where $\gamma_{SE} = k_{SE} n_{Rb}$ is the inverse of the spin-exchange time constant and depends only on the rubidium density n_{Rb}, and Γ is the intrinsic ^{3}He relaxation rate due to the cell wall, impurities, etc.

$$P_3(\infty) = P_{Rb} X_{cell} \frac{\gamma_{SE}}{\gamma_{SE} + \Gamma}, \tag{15}$$

where P_{Rb} is the rubidium electron polarization, which may be zero. The factor $X_{cell} \leq 1$ accounts for the observed reduction in ^{3}He polarization that varies from cell-to-cell but is not currently completely understood[39].

Apparently, $P_3(\infty)$ changes when the beam is on or off on a time scale that is short compared to 12 hours, and the most likely cause is that P_{Rb} is reduced by about 10-15% in the neutron beam. We speculate that this may be due to a distribution of static charge that forms with the beam on due to the ^{3}He(n,p)^{3}H reaction, similar to the ionization effect we observed in the early days of developing ^{3}He targets[40].

The summer 2007 LANSCE run was dedicated in part to direct measurement of the rubidium polarization in the neutron beam. To measure the P_{Rb}, we developed a standard electron-spin resonance (ESR or double resonance) experiment, measuring the intensity of transmitted optical pumping light as RF was applied and the magnetic field swept over a few-tenths of a Gauss in the range of 30 Gauss. The ESR spectra for two neutron beam intensities and no beam are shown in Figure 13. The ratio of adjacent peaks is directly related to P_{Rb}. The results for the relative polarization (fraction of the polarization for no beam) are shown in Figure 14. The results show that there is definitely an effect of the neutron beam on P_{Rb} that is consistent with the size of the effect observed with ^{3}He shown in Figure 12. The effect seems to be saturating as the neutron flux increases. The saturation is quite unexpected. Initial results from ILL seem consistent with this saturation, even at 10-20 times greater fluxes. Such a saturation could occur if the "poison" produced by ionization recombines at a rate proportional to the ionization rate.

There are several potential approaches to addressing and mitigating these observed effects. The double cell configuration, now used universally in electron scattering targets[41], may be adapted to the neutron spin filter. Improvements are also likely with hybrid Rb/K cells and with innovative laser technology. External cavity diode laser array bars, which produce about 15-20 watts of light over a narrower wavelength band than the Coeherent systems, have been developed and ILL [42] and studied with $\vec{n}+p \rightarrow d+\gamma$ cells at NIST. It has been shown that slightly higher polarization with much less laser power is generally achieved by using an external cavity bar in combination with the Coherent system. It is now possible to engineer a more stable external cavity laser, and recent commercial developments, including folded cavities and the use of volume Bragg gratings are promising. New cell designs will also

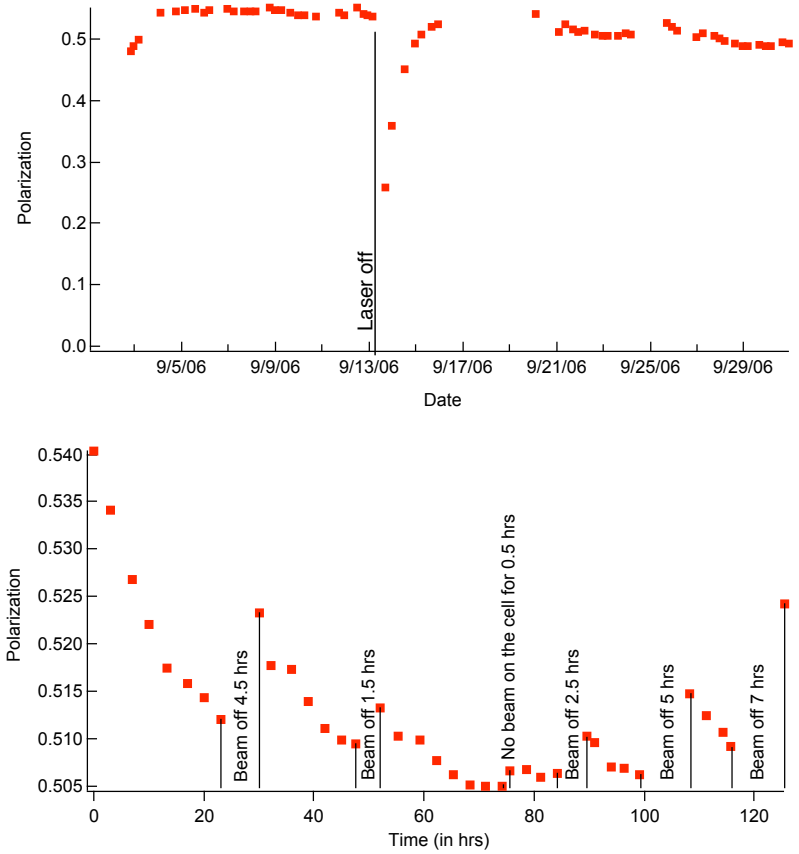

Figure 12: Neutron spin filter ^{3}He polarization over time. The top panel shows the long term behavior with a hint of decreasing polarization, possibly due to the white deposit on the cell surface. The bottom panel shows the effect of the neutron beam, which causes behavior consistent with a rapid decrease or recovery of rubidium polarization.

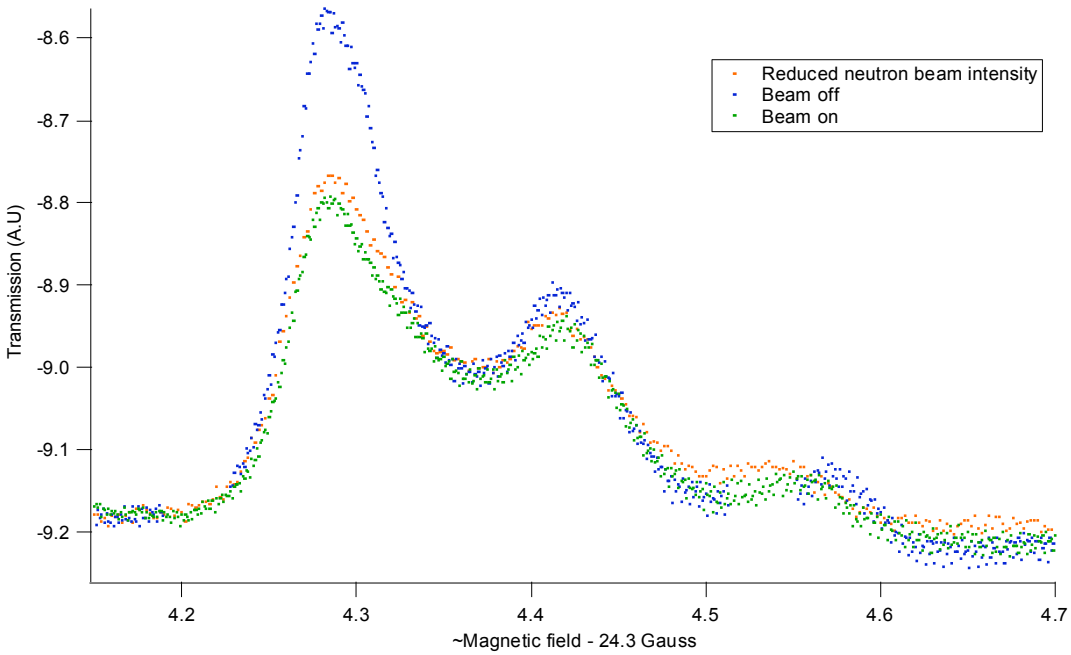

Figure 13: ESR spectra. For $P_{Rb} = 1$, only the largest peak would appear and for P_{Rb}=0, all peaks would appear with intensities given by the spin sequences.

be explored. In particular, we plan to adapt and test cells constructed of silicon windows attached to glass cylinders like thoise used at ILL[43]. These are commercially available from Hellma.

In summary, we are confident that the requirements for the neutron polarimeter have been met and demonstrated by the$n + p \rightarrow d + \gamma$ ^{3}He spin filter at LANSCE; however it is not yet clear that the ^{3}He spin filter will be practical as the primary polarizer. Addressing the ^{3}He problem is our highest priority, but it is premature to anticipate the solution. Thus our current efforts are focused on the following:

1. Continue systematic study of the time dependence of the short time constant polarization decay: how does it depend on neutron flux, cell temperature, laser power, and other parameters at ILL.
2. Address the milkiness.
3. Correlate the milkiness with either temperature or neutrons or both.

4.4 Spin Flipping and Spin Transport

The neutrons emerge from the ^{3}He spin filter with spins aligned with (or opposite) the magnetic field, and are transported to the spectrometer through the spin-flipper, and beyond the spectrometer to an analyzer and beam-dump. Ideally the neutron polarization remains constant in magnitude, the spin flipper rotates the polaization by exactly 180°, and the spins are transported to the analyzer without perturbation. Additionally, spin-state dependent forces, i.e. Stern-Gerlach type forces due to magnetic

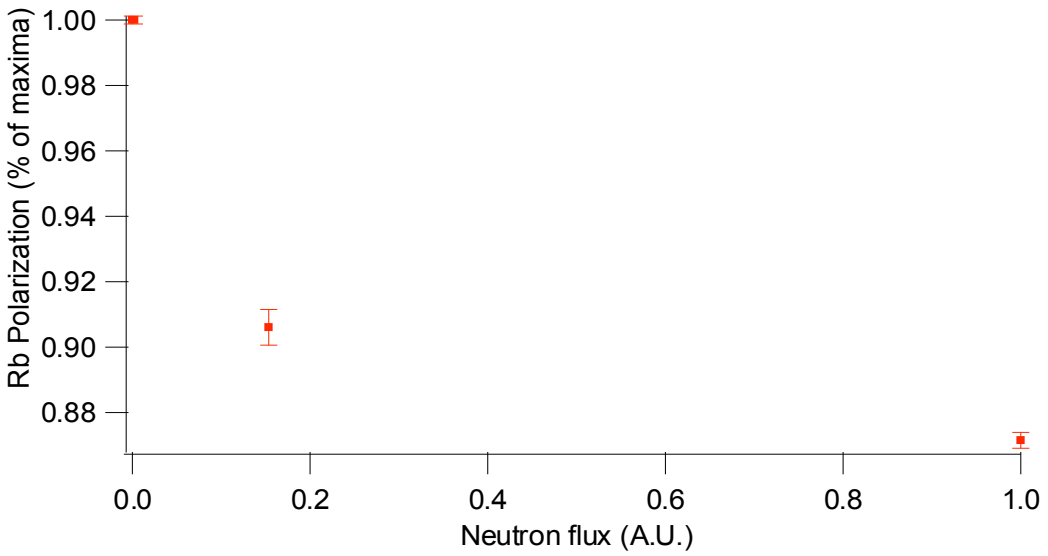

Figure 14: Relative rubidium polarization as a function of neutron flux. The maximum absolute P_{Rb} (no beam) is about 65%.

field gradients on the neutrons, must be well understood. In general, neutron spins are free, with only magnetic interactions. The equation of motion for a free neutron spin is

$$\frac{d\vec{\mu}}{dt} = \gamma_n \vec{\mu} \times \vec{B}, \tag{16}$$

where γ_n is the neutron gyromagnetic ratio. This is equivalent to the Bloch equation with no relaxation. For a two state system, i.e. spin 1/2, such as the neutron, the quantum mechanical result is equivalent.[1]

The most trivial case is a magnetic moment $\vec{\mu}$ along $\vec{B} = B_0\hat{z}$, with B_0 constant: then $\frac{d\vec{\mu}}{dt} = 0$ and $\vec{\mu}$ is constant. Consider what happens when $\vec{B}$ changes, for example due to neutrons propagating through a magnetic field gradient. In this case, the transverse components of $\vec{B}$ change and $\frac{d\vec{\mu}}{dt} \neq 0$. In the adiabatic limit, the rate of change of direction of the external field is much smaller than the Larmor frequency $\omega_L \approx \gamma B_z$, and the spin remains nearly perfectly aligned with $\vec{B}$. For neutrons with velocity $\vec{v}$ we can define an adibaticity parameter:

$$\alpha = \frac{\vec{v} \cdot \vec{\nabla} B_T}{\gamma_n B^2}. \tag{17}$$

Integrating the equation of motion over time gives the effective loss of static polarization along $\vec{B}$, i.e.

$$\cos\theta = \frac{(\vec{\mu} \cdot \vec{B})_f}{(\vec{\mu} \cdot \vec{B})_i}. \tag{18}$$

[1]The Bloch equations generally include relaxation terms due to material effects, i.e. a spectrum of magnetic field fluctuations due to neighboring spins (T_2 relaxation) and exchange of energy between magnetic and kinetic energy (T_1 relaxation). For a free neutron these terms are not relevant and relaxation has no meaning.

Through numerical integration we can accurately predict the effect of any field profile and set the tolerances on the magnetic field. For example, we require $(1-\cos\theta) < 10^{-4}$. With v=1000 m/s, and $B = 0.1$ T, a linear gradient must be less than about 0.3 T/m, which is not difficult to accomplish.

Similar considerations apply to spin flipping. The most effective neutron spin flipper is an adaibatic passage (AFP) flipper in which the neutron spins propagate through a constant RF magnetic field with a magnetic field gradient as shown in Figure 5, such that the Larmor frequency is far above resonance as the spins enter the RF field and far below the Larmor frequency as the neutrons exit the RF field. The RF field in spin-flipper coil is switched on to flip the spins and to a dummy load/coil to allow the spins to propagate unflipped. Such devices are routine for cold neutrons[44], and we have extensive experience with NMR, spin flipping, and modeling neutron spin transport, in particular for the emiT experiment[5, 6]. The RF spin flipper can be activated so that the spin can be flipped every SNS pulse, i.e. at 60 Hz.

Actually, the spin flipper rotates the neutron polarization by a neutron velocity dependent set of angles that can be described by cylindrical coordinates $\theta(\lambda)$ and $\phi(\lambda)$). As the neutrons propogate, the neutron spins precess about the 2-T guide field at a rate $\dot{\phi} \approx 4\times10^8$ rad/mm, and ϕ is quite effectively averaged. Thus the spin flipper can be accurately characterized by appropriately averaging $\theta(\lambda)$, i.e. $R =< \cos\theta(\lambda) >$. Ideally $R(\lambda) = -1$. The quantity $1 - R$ is generally called the spin-flip efficiency.

If the ^{3}He spin filter is used, the neutron spin can also be reversed by reversing the ^{3}He polarization with adibatic fast passage (AFP) NMR. Losses on the order of 0.1%or less per flip are routine. AFP on the ^{3}He is generally slower than RF spin flipping; however tailoring the RF pulse in amplitude and frequency can reduce the losses by orders of magnitude[49]. When flipping the ^{3}He spin, the circular polarization of the light must also be reversed by changing the $\lambda/4$ plates. With liquid crystal polarizers, the ^{3}He spin can be flipped every second or even more frequently if necessary.

4.5 Neutron Polarimetry

Precision measurement of the correlation coefficients requires that the neutron polarization be accurately determined for both spin states (parallel and opposite $\vec{B}$), that is both the neutron polarization and the spin-flip efficiency must be meaured. For PANDA, we will use a thick ^{3}He spin filter. The principle of polarimetry is wavelength dependent measurement of the transmission through a ^{3}He filled analyzer cell which was originally characterized with $P_3 = 0$, i.e. unpolarized ^{3}He. The ratio

$$[\frac{T_A^P}{T_A^0}] = \cosh(P_A\sigma_0 t_A\frac{\lambda}{\lambda_0}) + P_n(\lambda)\sinh(P_A\sigma_0 t_A\frac{\lambda}{\lambda_0}). \tag{19}$$

Here T_A^0 and T_A^P are the transmission with the analyzer unpolarized and polarized, respectively. The ^{3}He polarization in the analyzer can be reversed by AFP NMR with losses much less than 0.1%[49] so that we can effectively let $P_A \to -P_A$ in equation 14, and the polarimetry asymmetry formed:

$$\frac{[T_A^P/T_A^0]^+ - [T_A^P/T_A^0]^-}{[T_A^P/T_A^0]^+ + [T_A^P/T_A^0]^-} = P_n(\lambda)\tanh(P_A\sigma_0 t_A\frac{\lambda}{\lambda_0}). \tag{20}$$

The important point is that $\tanh(P_A\sigma_0 t_A\frac{\lambda}{\lambda_0})$ can be made as close to unity as desired by tuning the analyzer ^{3}He thickness, t_A, for any polarization P_A. This is the principle of the opaque analyzer. The cost is reduced transmission through the analyzer, however a significant fraction of the entire neutron beam will be transmitted through the analyzer so neutron statistics will not be a practical limitation. The neutron beam transmitted through the analyzer cell will be measured with a position sensitive

detector, providing useful information on polarization and intensity variations across the spectrometer aperture.

As noted in Section 4.4. the spin flipper actually rotates the spin of a neutron by an angle that depend on the neutron velocity and wavelength. The effect on the polarization expressed in terms of R=$< \cos\theta(\lambda) >$. We can express the effect on the polarization as

$$P_n^- = (1 + 2R(\lambda))P_n^+ \tag{21}$$

Recall that $< \cos\theta(\lambda) > \approx -1$, i.e. $\theta = \pi - \delta$, so that $P_n^- \approx -P_n^+(1 - \bar{\delta}^2)$. The spin flip efficiency is

$$\mathcal{F} = 1 - \frac{\bar{\delta}(\lambda)^2}{2}. \tag{22}$$

We expect $\bar{\delta}^2$ to be 10^{-4} or less. The principle of PANDA is to directly measure the neutron polarization in both spin states, i.e. i the spin flip efficiency will not enter directly into the analysis. We plan to use the ^{3}He density and polarization as "knobs" to vary the opaque wavelength range of the neutron-polarimeter ^{3}He cell and thus to directly calibrate our measurement of the relationship given in equation 23. A refillable, single ^{3}He cell can be used to provide a variable opacity.

The development of the $n + p \rightarrow d + \gamma$ experiment gave us the opportunity to study the principle of this approach to polarimetry by measuring the transmission of *unpolarized* neutrons through polarized ^{3}He[11]. Though the $n + p \rightarrow d + \gamma$ set-up was not optimized in terms of backgrounds, neutron polarimetry at the sub 1% level (a few $\times\ 10^{-3}$) was achieved by measuring the transmission through the ^{3}He with a pair of thin $(1/v)$ monitors, M1 upstream of the ^{3}He polarizer cell and M2 downstream. Assuming that ^{3}He dominates the wavelength dependence of neutron capture, the signal in the downstream monitor (M2), corrected for backgrounds, is given by

$$M2(\lambda) = A * M1(\lambda) \exp(\alpha\lambda) \cosh(\alpha\lambda P_3), \tag{23}$$

where $M1$ is the background corrected signal from the upstream monitor, which is used to normalize any changes in the neutron spectrum. The factor A accounts for efficiencies, gains and wavelength independent attenuation, α is the ^{3}He attenuation coefficient for $\lambda = 1$ Å, and P_3 is the ^{3}He polarization. With a separate measurement of the ^{3}He thickness, also possible with the neutron beam, the ^{3}He polarization can be extracted. The neutron polarization is

$$P_n(\lambda) = \tanh(\alpha\lambda P_3). \tag{24}$$

This technique was used for the ^{3}He polarization data shown in Figure 15. In the left panel, we show the ratio $M2(P)/M2(0)$, where $M2(P)$ is measured with the ^{3}He polarized, and $M2(0)$ is measured with the ^{3}He unpolarized. The ratio is fit to the function $\cosh(\alpha\lambda P_3)$, and the residuals are a few$\times 10^{-3}$. In the right panel, we plot $P_n^{\rm nom} = \sqrt{M2(0)^2 M2(P)^2 - 1}$ as a function of λ and a fit to the $\tanh(\alpha\lambda P_3)$, again showing that the residuals are significantly less than 1%. The residuals do indicate a systematic effect, which has been studied with simulated backgrounds, and we conclude that with effort, the backgrounds in the monitors can be reduced sufficiently for sub-0.1% measurement of the neutron polarization. An additional advantage provided by the time-of-flight analysis is that this dependence is a strong discriminator for backgrounds and other systematic effects.

It is not necessary that the analyzer ^{3}He cell be thick for all relevant neutron wavelengths, only that it be sufficiently thick at wavelengths where sufficient neutron flux is available to calibrate the analyzer thickness and polarization. It is practical to choose the ^{3}He thickness of the analyzer so

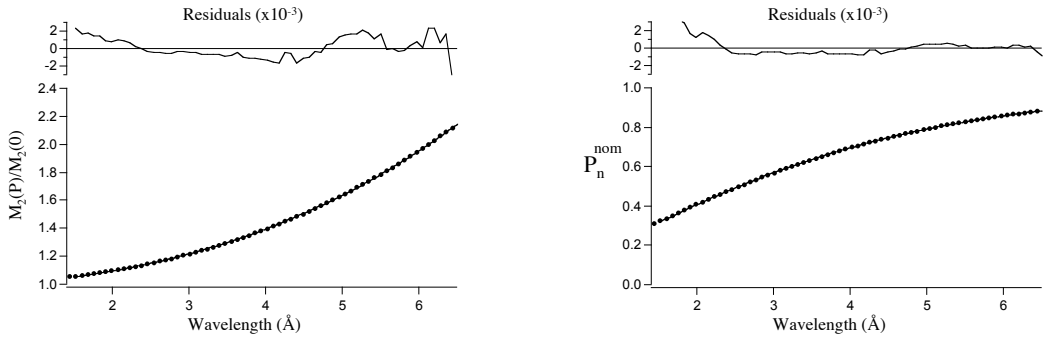

Figure 15: Left: the ratio $M2(P)/M2(0)$ (circles) and fit to $\cosh \alpha\lambda P_3$ (solid line) with residuals. Right: The nominal neutron polarization $P_n^{\rm nom}$ (circles) and fit to $\cosh \alpha\lambda P_3$ with residuals.

that $A_n > 99.9\%$ and the time to achieve a statistical error on $P_n A_n$ is reasonable. With P or A separately determined, the neutron polarization and spin flip efficiency can be determined with high precision. We emphasize that with the pulsed SNS-FnPB beam, the velocity discrimination will allow us to monitor the neutron polarization and spin flip efficiency in real time, for example to account for changing polarization ^{3}He in a spin-fliter polarizer.

4.6 The PANDA Spectrometer

The spectrometer has a uniform magnetic field of nominally 2 T and electric fields tailored by a set of five-electrodes. The anticipated field layout is shown in Figure 6. Five electrodes will be used to confine and accelerate the protons or provide an electrostatic mirror at either end of the spectrometer. The electrostatic retarding potential V_0 will be used to measure the integrated proton spectrum above eV_0. Proton energy resolution will allow us to study systematic effects, proton energy dependent corrections, and possible new physics that would depend on recoil energy as shown in Figures 3 and 4. The spectrometer described above does provide proton energy measurement, however only the longitudinal component of the proton momentum is analyzed by the electric field E_z. The electrodes can also be set to make an electrostatic mirror for the protons at either end. This will be used to study backgrounds and spectrometer analyzing power.

In the 2 T magnetic field, charged particle orbits have radius up to 2 mm, thus the 2.6 cm detector aperture will limit the size of the fiducial volume viewed by the detectors. Ideally, the spectrometer should have 100% efficiency for neutron decays, however the neutron beam can only be collimated in the x and y directions (z is along the neutron beam). Thus some kind of proton collimation is needed, at least in the z direction, i.e. along the beam. If charged particles do miss the detector active area, it is important to consider where they go and, in particular if they produce background, and more importantly if the backgrounds are the same for the ends of the spectrometer. Note that the electrostatic potentials shown in Figure 6 obiously lead to trapping of low-energy electrons from neutron decay and from the ionization of the residual gas. These effects are discussed in Section 5.

Simulations have been used to study the details of the detector design. Particle orbits in the spectrometer were tracked by 4th order Runge-Kutta integration. These simulations have been used to determine the efficiency based on beam size, magnetic field strength, variations and asymmetries in the efficiency due to magnetic field imperfections, and will be used to predict backgrounds due to charged

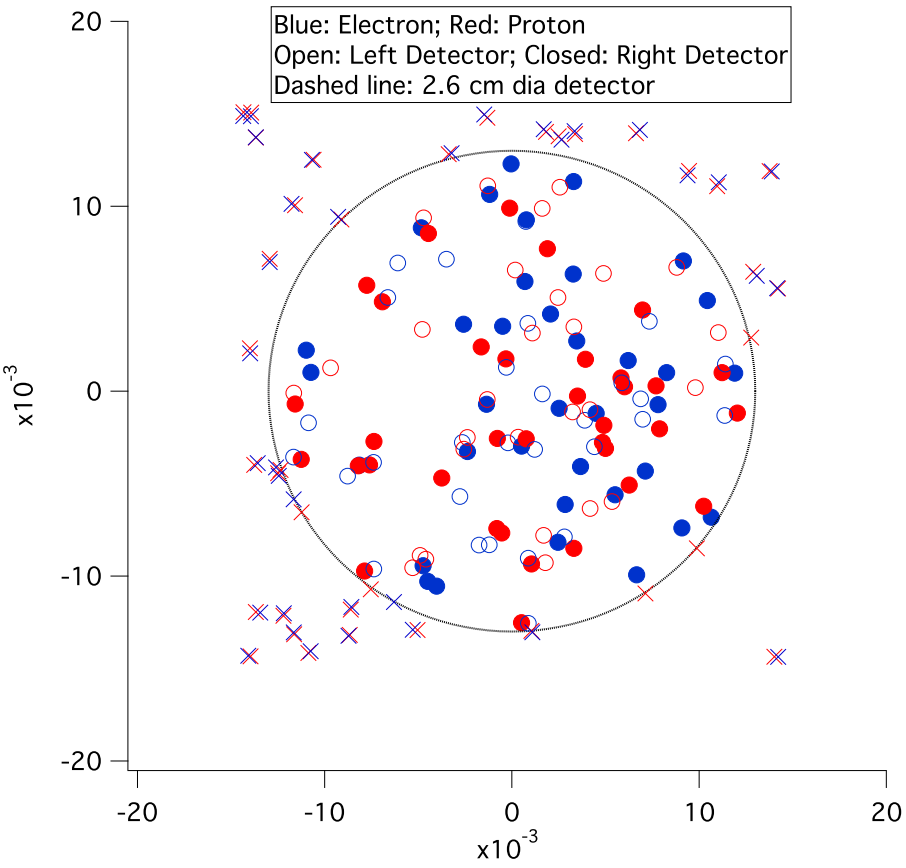

Figure 16: Simulation results for events incident on SBD for 3 cm diameter beam and 4 T field. Circles are hits, X's are misses, blue are betas and red are protons. The efficiency is 59%.

particle scattering from spectrometer baffles and other spectrometer elements. In Figure 16, we show a set of events incident on the 600 mm^2 face of the SBDs. Events that would miss the detector should be collimated by baffles to prevent backgrounds and misidentified events so that they do not produce background.

4.7 Detectors

PANDA is based on the use of commercially avaialable silicon detectors. The current design is based on ORTEC 600 mm^2, 1mm thick surface barrier detectors (SBDs). The cost is \$6500 Each. An electron-proton coincidence event from the RDK experiment is shown in Figure 17. The small proton signal is delayed and significantly above the noise. The electron energies will vary from event to event, but the proton signal is constant because the proton energy is determined by the nominally 30 kV accelerating field. Note that a 10 bit ADC was used for data acquisition. PANDA will use 14 bit ADCs.

Detector tests with low energy protons will be very useful for development purposes. We have developed a low-cost proton gun based on the quadrupole mass spectrometer in a commercial residual gas analyzer. This test set-up that will be completed and used for the PANDA SBDs as well as a variety of studies of backgrounds etc.

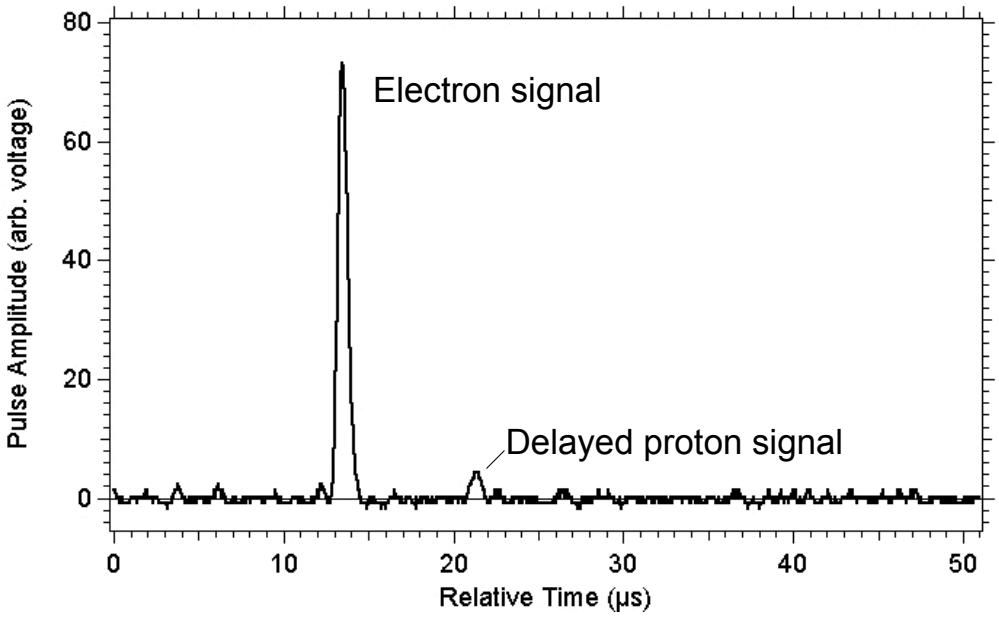

Figure 17: Silicon barrier detector signal triggered by the electron signal, showing the delayed proton signal from the RDK experiment. For these data, the resolution was limited by the 10 bit ADC. For PANDA, 14-16 bits will be used.

4.8 DAQ

We anticipate using a set-up similar to that developed for the 2nd generation Radiative Neutron Decay experiment (RDK). The DAQ consists of triggered waveform acquisition for all channels. We will use 14 bit ADCs, which will provide 16× better amplitude resolution than shown in Figure 18. Each event will be triggered by a single pulse with slope and amplitude above threshold. The waveforms for the two detectors, spin flip information, ^{3}He information as well as all monitors (magnet currents, voltages, leakage currents, temperatures, magnetic fields, etc.) will be stored for each event. As in the radiative neutron decay experiment, pulse-height windows for the electron and proton can be set for the silicon detectors, and the coincidence requirement simply reduces backgrounds.

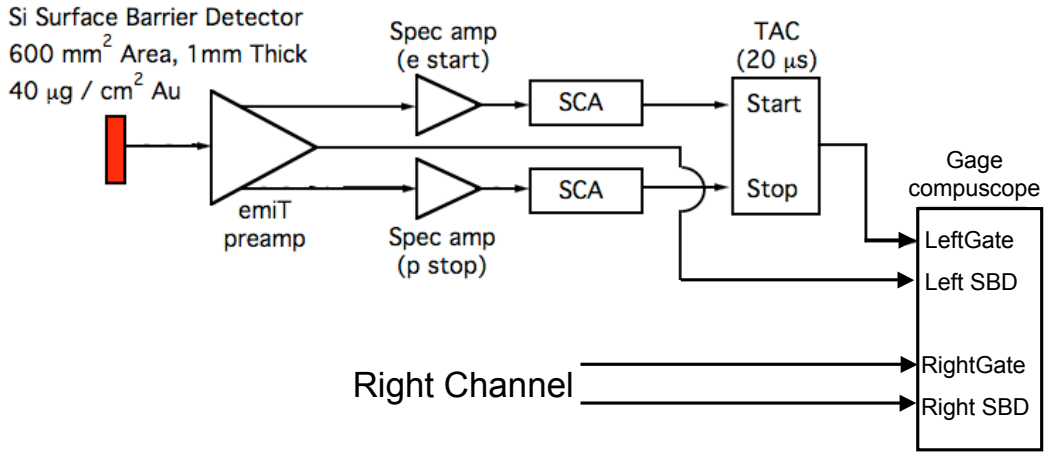

Figure 18: DAQ set up for each SBD, similar to that used for the RDK experiment.

4.9 Spectrometer Magnet

The PANDA experiment requires a nominally uniform field. The experiment will detect decays at a rate of about 1 Hz/cm$^3 * V_d$, where V_d is the decay volume visible to the SBDs. This volume depends strongly on the magnetic field, because the radii of the beta and proton cyclotron orbits are inversely proportional to the field. In Figure 19, we show the total count rate and statistical error for one month of running as a function of magnetic field strength. The nominal field for PANDA@SNS is 2 T.

The magnteic field profile also affects systematic errors, in particular protons that are reflected from "bumps" in the B-field can be detected in the wrong detector and betas that are not detected or are lost due to bottle effects can produce an asymmetry in the efficiency for the two directions. These are discussed in Section 5.

The common-beta-decay-magnet design concept has moved forward. We have compiled the requirements of the experiments and provided a baseline design that was discussed in a presentation to a potential vendor (AMI of Oak Ridge). The magnetic field profiles for the three experiments are shown in Figure 20. All three experiments require a uniform field in the decay region. This will be produced by a split-coil pair. The magnetic field in the decay region is transverse to the neutron beam. PANDA requires a nominally uniform magnetic field over a drift region of about 1 meter on either side of the

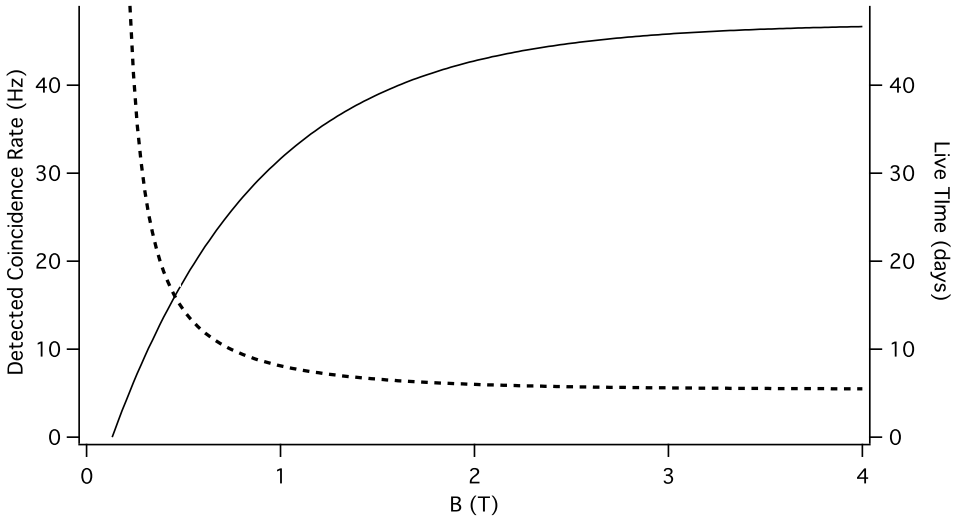

Figure 19: Total count rate (solid line) and live-time (dashed line) for a 10^{-3} statistical error on C for a beam 10 cm tall (along the spectrometer axis) and a function of the strength of the uniform magnetic field. The width of the beam (transverse to the spectrometer axis) can be increased for larger magnetic fields due to the smaller cyclotron orbits. A decay rate density of 1 Hz/cm^3 and an average neutron polarization of 85% are assumed.

decay region, which will be produced by a split coil and two solenoid windings, while Nab and abBA require a field reduction (field-line expansion) to allow time-of-flight analysis of the proton energy as discussed below. For PANDA, only the z-component of momentum can be analyzed by electric fields. One important feature is the cold bore with load locked access for each experiment's detector packages. With the common magnet facility, each experiment can be independently developed and optimized. Simulations using common magnet PANDA configuration are ongoing, for example we are considering alternative designs compatible with the common magnet coil configuration. An example that has no minima between the center and the SBD detectors is shown in Figure 21. A final design of the magnetic fields will require complete simulations of the experiment as discussed further in Section 5.10.

The common spectrometer magnet is the best approach to the overall program of PANDA, abBA and Nab; however we consider the penalty of using a conventional (non-superconducting magnet) and the use of existing magnets, in particular with the neutron beam along the nominal magnetic field axis (e.g. like the Sussex/NIST lifetime magnet). From Figure 19, it can be seen that the impact of reducing the field to 0.1 T is an intolerable reduction in count rate.

4.10 Vacuum Requirements

Vacuum residual gas (H_2 at UHV) affects backgrounds, discharges, component performance and the spectrometer analyzing power. These are discussed in separate part of Section 5. Our goal is 10^{-9} torr. This seems attainable with the cold bore or cryopumped spectrometer, though careful design of feed-throughs, materials and the neutron windows will be essential. A great deal of effort will need to go into designing and attaining this vacuum in the PANDA spectrometer

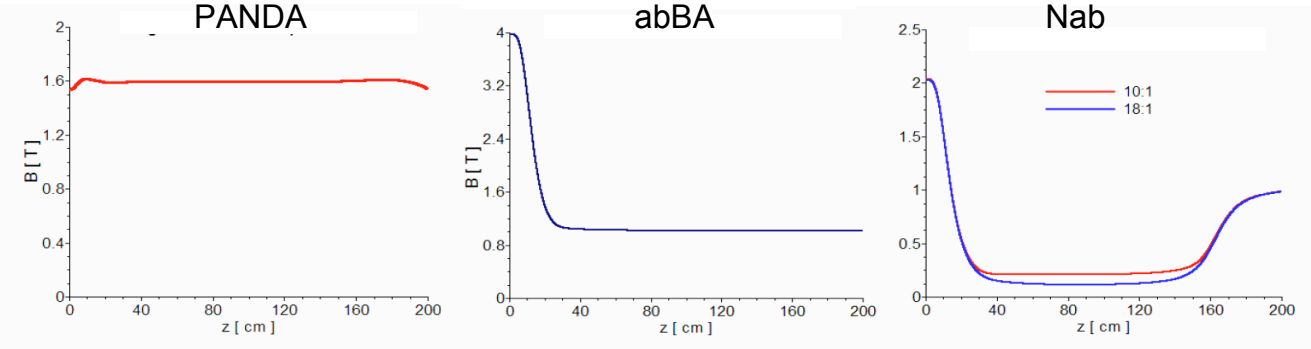

Figure 20: Magnetic field profiles calculated for the fist pass study of a multiple coil set-up envisioned for the FnPB Beta-decay magnet facility. The three configurations correspond to the PANDA, abBA and Nab experiments.

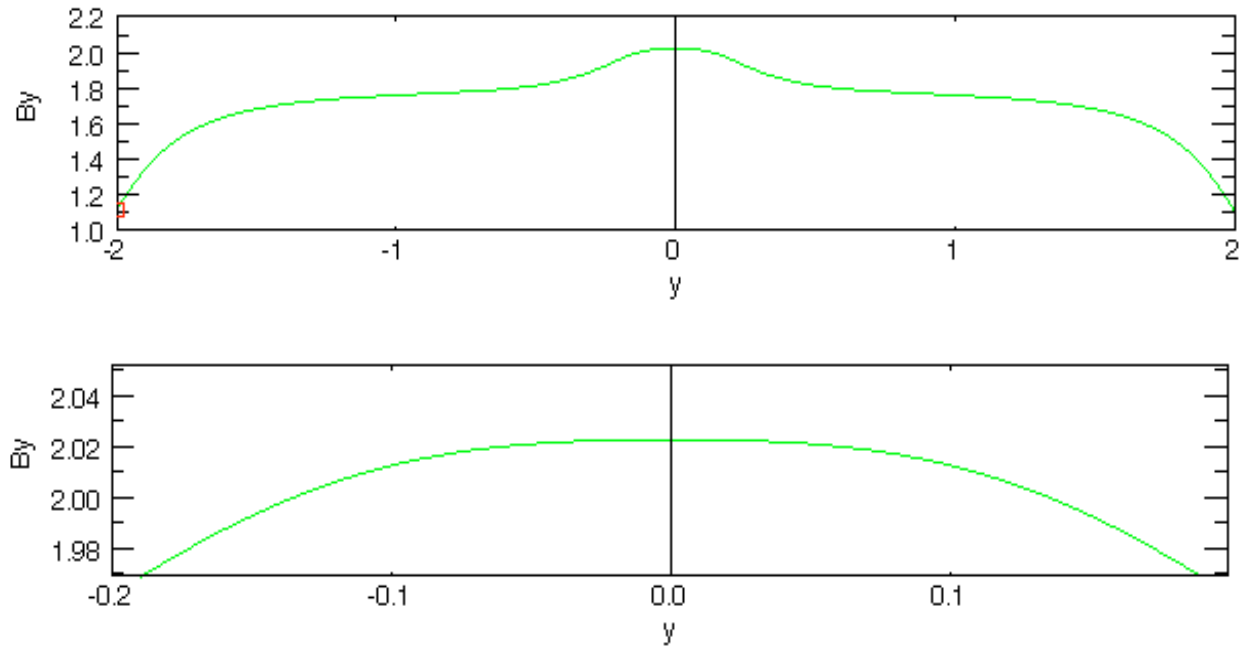

Figure 21: Magnetic field profile along the spectrometer axis produced with split solenoids developed for PANDA so that there is no minimum in the decay volume (see Figure 6 for field profiles along the neutron beam). The bottom panel shows the field on a finer scale.

4.11 Analysis

The proton-asymmetry is defined in equation 2; however we need to account for spin-dependent systematic errors (false asymmetry) that would arise from effects such as backgrounds produced by polarized neutrons, Stern Gerlach effects etc.

$$A_p = \frac{N_+ - N_-}{N_+ + N_-} = kC\mathcal{A}\mathcal{F}(1-f)P_n + A_{false}, \tag{25}$$

where N_+ and N_- are, respectively, the number of protons per neutron decay emitted with $\hat{\sigma}\cdot\hat{p}_p > 0$ and $\hat{\sigma}\cdot\hat{p}_p < 0$, P_n is the appropriately averaged neutron polarization, $\mathcal{A}$ is the analyzing power for proton detection, $\mathcal{F}$ is the neutron spin-flip efficiency, and f is the fraction of $(N_+ + N_-)$ due to backgrounds. For C, k is a kinematic parameter that depends on the range of the proton energy spectrum that is measured. For each retarding voltage, k will determined by Monte Carlo simulation, which includes the acceptance for electrons and protons.

The principle of the analysis is straight forward: determine $N_\pm$, correct for additive errors (A_{false}) and for multiplicative errors ($\mathcal{A}$, $P_n^\pm$), and the background fraction f and the kinematic range detected. The kinematic range will be determined by the retarding voltage and electrode positions with respect to the magnetic field variations, and will require a combination of monitoring and checks.

Extracting physics from C requires accurately accounting for corrections due to coulomb, recoil and radiative effects. For the proton asymmetry, these corrections have been calculated by Gluck[2, 3] (see also [21] for recoil corrections). To be able to compare results of the proposed experiment with the precise measurements of other angular asymmetries in neutron decay it is desirable to use calculations of radiative and recoil corrections for all observables in the same approach, to keep possible theoretical uncertainties under control. These calculations have been done recently in effective field theory [20, 22] and they resulted in the exact and complete Standard Model description with only one free low energy constant (LEC). This provides a complete description of angular correlations in neutron decay with an accuracy of about 10^{-5} (provided the LEC is obtained from a complementary experiment or estimated). To present results of these calculations for C in terms of variables used in this proposal some kinematic calculations are required. These calculations are underway[23].

5 Systematic Effects

Equation 25 shows that a 0.1% measurement of kC requires backgrounds, analyzing power, neutron polarization, and neutron spin flip efficacy be known to much better than 0.1%. Extracting physics from kC also requires precise determination of the kinematic range of protons AND electrons detected. The kinematics depend on the spectrometer fields including field imperfections, charge trapping, etc.

There are also potential effects that couple polarization to backgrounds and analyzing power. For example the neutron beam position and polarization distribution depend on the spin direction due to Stern Gerlach effects. This can affect the polarimetry/spin flip efficiency measurement, backgrounds AND the spectrometer analyzing power. The most challenging issues will be accuracy of polarimetry affected by the spin transport from the spectrometer to the neutron polarimeter, neutron polarimeter backgrounds and the spectrometer analyzing power.

The PANDA experiment aims to build an recent experience at each stage. Our recent experience includes the RDK experiment, neutron polarimetry measurement with the $n + p \rightarrow d + \gamma$ set-up at LANSCE and the emiT experiment. The emiT experiment is sensitive to asymmetries at the few$\times 10^{-4}$ level, well beyond the sensitivity of any other neutron decay experiment. Our experience convinces

us that a three pronged approach is essential to addressing systematic effects. In our approach, we **M**inimize the problems, **M**easure their effects directly, **M**ake minimal corrections based on detailed understanding of the apparatus, the physics and modeling. In this section, we describe the **MMM** strategies developed to address these effects.

5.1 Polarization and Spin Flip Efficiency

PANDA will directly measure the neutron polarization in BOTH states of the neutron spin flipper by measuring the transmission of neutrons through an opaque ^{3}He analyzer. In section 4.5 we describe the plan to employ AFP flipping of the analyzer ^{3}He spin. In Figure 15, we show that our analysis of the time-of-flight dependence of neutron transmission through ^{3}He produced residuals at the 10^{-3} level. Backgrounds in the neutron monitors could produce these residuals, and backgrounds will likely be the ultimate limit to the precision of polarimetry for PANDA. Our strategy for Modeling, Minimizing and Measuring these backgrounds takes advantage of the time-of-flight/wavelength dependence as described below.

Neutron spin flipping with an adiabatic passage flipper and adiabatic neutron spin transport with much better than 0.1% precision have become routine[44]; however this must be measured. In the PANDA approach, the spin flip precision does not directly enter because we will measure the neutron polarization in both spin states. Alternatively, this can be viewed as directly measuring the spin flip efficiency $\mathcal{F}$. The precision of polarimetry will also be limited by the precision of the neutron spin transport between the detector fiducial volume and the neutron polarimeter. Once the final magnetic field configuration is established, we will calculate the neutron spin transport for all trajectories by integration of the Bloch equations (i.e by Runge-Kutta) using the routines developed for emiT, and shim the field as needed to keep the effects at the 0.01% level. In development runs, we will directly measure the neutron polarization with polarimeters (i.e. ^{3}He analyzer cells) UPSTREAM and DOWNSTREAM of the spectrometer. This will require the same attention to backgrounds in the the UPSTREAM polarimetry position.

It is important to carefully control the magnetic fields, and to ensure that changing the spin flipper state does not affect the detectors. The use of a polarized ^{3}He spin filter, discussed below, provides an additional "flip" that would allow direct measurement of systematic effects related to spin flipper noise.

5.2 Stern Gerlach effects

Magnetic field gradients in the neutron spin transport field will lead to deflection of the neutron beam that is spin dependent. The transverse Stern-Gerlach effect will lead to a deflection over a distance L given approximately by

$$.\theta_{\pm} \approx 3 \times 10^{-7} \nabla_{\rho} B_z L \ \text{ rad} \tag{26}$$

For B_z in Tesla. This will lead to a change the beam position by a few microns, which could, in turn change the average density and decay rate in the spectrometer fiducial volume by as much as a few $\times 10^{-4}$, assuming the neutron beam intensity changes by 100% over 10 cm. Defelction due to the transverse Stern Gerlach effect can also affect polarization gradients across the neutron beam. These are discussed in the next section. The longitudinal Stern Gerlach effect will lead to a spin dependent change in neutron velocity by a fraction

$$\frac{\Delta v_z}{v_z} \approx 6 \times 10^{-7} \nabla_z B_z L, \tag{27}$$

leading to a spin-dependent change of density and decay rate of order 10^{-6}.

5.3 Polarization position dependence

We can expect the neutron polarization to vary across the neutron beam. For the ^{3}He polarizer, this will arise due to any variation in wavelength for the beam emerging from the FP13 guide and due to variation in the thickness of ^{3}He. For the XSM, crossed supermirror polarizer, the polarization is expected to vary as well, though much less than for the single supermirror polarizers.

Systematic effects that will arise due to position dependence are first order and second order. First order effects include knowing the correctly averaged neutron polarization in the fiducial volume. Second order effects include coupling to the position dependence of spectrometer efficiency and analyzing power. We will measure the first order polarization variation directly with the neutron polarimeter. The position dependence will be studied with collimation beginning just downstream of the polarizer so that individual portions of the beam in the neutron fiducial volume can be isolated. The neutron polarimeter will be position sensitive, and the fiducial volume will be mapped to the polarimeter position.

5.4 Wavelength and time-of-flight dependence

The principle of opaque ^{3}He polarimetry is discussed in Section 4.5. For long wavelengths, the analyzing power approaches unity. Time of flight provides accurate wavelength determination with wavelength dependent time resolution limited by smearing of the initial neutron pulse over time of about 0.25 ms, the moderation time. There is also position dependence due to the 30 cm moderator size as well as path-length variations for different neutron trajectories through the guide. These finite-time-resolution effects do not alter the effectiveness of the opaque anlayzer, however there are two effects that could confound the relation of wavelength and time-of-flight: backgrounds and delayed neutron emission from target spallation and fission products. For both of these effects, faster neutrons can arrive later than L/v due to longer path length (for background neutrons scattering from the cave walls) and due to delayed emission.

Reducing backgrounds of neutrons detected by the analyzer monitors to below the 10^{-3} level will be challenging but achievable. The design of the experiment will minimize backgrounds by modeling the entire beam line and apparatus (e.g. using MCNP and GEANT4) as well as empirical background studies. Backgrounds, in particular time-of-flight dependent backgrounds in the analyzer detectors, will be measured by varying the collimation and shielding of the detector.

The spectrum of delayed neutrons will alter the relationship of wavelength to time-of-flight over the entire time-of-flight range. While this is expected to be well below 10^{-3} over the entire wavelength range, we will directly measure the neutron spectrum by measuring attenuation of the neutron beam through a variable pressure ^{3}He cell in the analyzer cell position, and also with varying collimation. The results from the thin detectors and the thick analyzer detectors must corroborate throughout the time-of-flight range.

5.5 Time Dependence

Time dependent effects will be very different for the ^{3}He polarizer and the XSM super mirror polarizer. For the XSM, we expect time variations only due to changes in the neutron beam flux (proton current, moderator conditions), guide field drifts and spectrometer drifts (e.g. detector temperatures). The ^{3}He is intrinsically unstable, and a ^{3}He spin filter polarizer will require a different strategy. The

spectrometer analyzing power is also expected to be time-dependent at some level due to wandering patch effects that change the electric fields. Backgrounds may vary with time as well.

In general, we will monitor the proton current, the neutron flux versus time of flight in the three monitor positions, spectrometer parameters and leakage currents.

5.6 Unpolarized runs

Runs with unpolarized neutrons can, in principle, be very useful to check a number of systematics. Most importantly the spectrometer analyzing power, and position dependent backgrounds can be accurately measured with unpolarized runs. With a ^{3}He-spin-filter polarizer, an unpolarized beam can be achieved by removing the ^{3}He cell or by depolarizing the ^{3}He. For the XSM crossed supermirror polarizer, the neutron beam is shifted and unpolarized runs are not practical. The XSM can be arranged so that the polarized beam is parallel to the incident beam, so it may be possible to develop a strategy for shifting the spectrometer. We have therefore developed an experimental strategy that does not rely on unpolarized runs.

5.7 Delayed protons

Protons from neutron decay are delayed with respect to the betas by a time denoted TEP. Monte Carlo results for the spectrum of proton delay times for a 1.8 T field are shown in Figure 22. Fewer than 0.1% of the events have delay times greater than 40 μs. Protons with long delay times have very small momentum components along the spectrometer axis and are also more likely to be reflected from magnetic field "bumps."

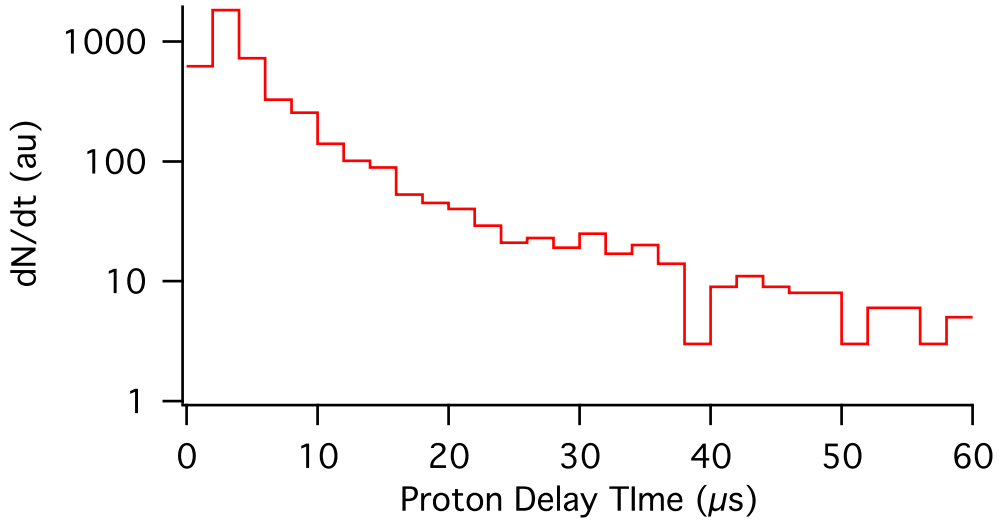

Figure 22: Spectrum of proton delay times from Monte Carlo studies of the PANDA spectrometer. The SBDs are 1 meter from the center of the spectrometer.

5.8 Backgrounds

Backgrounds are any detector coincidences within the beta-prpton timing window that are not primary products of decays of polarized neutrons in the detector fiducial volume. Backgrounds that affect the neutron polarimeter are discussed in sections 4.5 and 5.1. The effect of background is shown in equation 25, i.e. the factor the factor $(1 - f)$, which dilutes the asymmetry. Spin dependence of the background will also contribute to the false asymmetry A_{false}. Backgrounds must be reduced and understood to much better than 0.1% in order to accurately measure C. To begin, we have the experience of the the earlier experiments. In the RDK experiment with the CW beam at NIST $f < 1\%$ was demonstrated with electron-proton coincidences[10]. Shielding, and beam line design improvements are expected to improve this significantly for the next RDK run.

Anticipated sources of background are presented in Table 3. Backgrounds can be characterized first by whether they are present with the neutron beam on or off (BEAM). Position dependent backgrounds (POSN) will be different for the two SBDs. Time-of-flight (TOF) dependent backgrounds are any that originate from the neutron pulse and thus vary in any way over the TOF window for neutron decay. Beta-proton coincidences are correlated with a coincidence time (TEP) of 40-50 μs due to the drift time of protons along the spectrometer axis from the decay vertex to the HV acceleration gap. Within this TEP window, random coincidences appear as background that can be measured by examining the acausal TEP window at negative times. Neutron spin dependent backgrounds (SPIN) are essentially second order backgrounds that result from changes in the neutron beam intensity when the spin is flipped, e.g. due to Stern Gerlach (SG) deflection of the beam. Some backgrounds will deposit specific energy in the SBDs (SiE); for example cosmic rays are minimum ionizing and will deposit about 300 keV in 1 mm of Si, which falls in the window of energies of betas from neutron decay. Background events that originate within the spectrometer could arise from neutron decays, i.e. betas and accelerated protons scattering from baffles and collimators, accelerated residual gas ions, in particular due to Penning-trapped negative species near the center of the spectrometer that ionize the residual gas, neutrons scattered into the spectrometer and secondaries, i.e. Compton electrons from high energy gammas.

For example, the third line in Table 3 (Neutron Pulse) describes backgrounds caused by the incident neutrons scattering off collimators and neutron beam transport components and producing γs that reach the SBDs. This be absent in beam-off runs (BEAM-y). It will be position dependent and thus in general different in the two SBDs (POSN-y). It will have a TOF dependence that is different from that of neutron decays in the fiducial volume (TOF-y). It can be spin dependent if the neutrons scatter downstream of the polarizer and spin-flipper (TEP-y). It will in general deposit a continuum of energies in the SBD (SPIN-y) will not present a well difined energy deposition window in the DBDs (SiE-n). It will NOT change with proton acceleration HV (HV-n) and will NOT change with the proton energy analysis (KEProton-n). Some scattered neutrons can produce secondaries and charged particles, which could scatter from the vacuum residual gas (Pressure- y).

Several types of background can be produced by residual gas ions. These have been characterized as vacuum protons events observed in the NIST lifetime, emiT and RDK experiments. Residual gas ionization by Penning trapped negative ions can lead to significant backgrounds. For example, a neutron decay will produce energetic electrons, but with the field configuration shown in Figure 6, electrons with energy below 24 keV, about 2% of the neutron decay spectrum, will be trapped axially by the electric potential and confined by the magnetic field. These low energy electrons have a mean free path to inelastic collisions in hydrogen at 10^{-8} torr (10^{-12} gm/cm^3) of $\lambda_{fp} \approx 5x10^3$ m[45], *i.e.* about 10,000 times the length of the trap. These low energy betas travel that distance in the trap in about 100 μ s. Consequently, each neutron decay would produce on the order of 16 proton ions (2% of

24 keV/30 eV - the cost per ion pair). These would be accelerated and detected as background proton singles events. The vacuum proton background is strongly dependent on residual gas density and will be studied as a function of vacuum pressure, high voltage and neutron beam on/off. These effects will be addressed in more detail in the final design considerations.

A number of features of PANDA will reduce backgrounds to significantly below those of the RDK experiment. Direct measurements will reduce the uncertainty of f to well below 10^{-3}. Most importantly, PANDA is a coincidence experiment, i.e. we require two signals in the same or separate SBDs within a window of 20-40 μs; like RDK, energy windows for the beta and proton will also be set (see Figure 17). The SBDs will be one meter or more away from the beam and well shielded from the beam line components; time-of-flight will provide additional discrimination.

While the RDK experiment provides a reference for our goal of reducing the uncertainty in f well below 10^{-3}, we will develop the beam line and spectrometer with a design based on accurate modeling using MCNP and GEANT4 simulations of the all components of the beam and spectrometer. This will also provide time-of-flight dependent background information. We will, of course, also use an empirical approach, i.e. vary all the parameters listed as in Table 3. Shielding will be designed and empirically tuned to minimize any remnant problematic background sources, varying and turning off the proton acceleration high voltage, beam off runs and moving the 2 ms beam-off chopper interval through the time-of-flight window. Nevertheless, Table 3 shows that Scattered e-p, the background from a beta or proton from a neutron decay in the detector fiducial volume that is scattered from a spectrometer component, cannot be discriminated with any of the dependencies shown. This background does, however depend on the magnetic field strength and collimation and can be studied by varying these parameters.

Table 3: Background Sources and dependence on parameters measured in PANDA. The first line characterizes a true neutron decay coincidence event. Dependence on TOF will generally be different from Neutron Decay events and other sources such as scattered neutrons.

Source	BEAM	TOF	TEP	POSN	SPIN	SiE	HV	KEProton	Vacuum
Neutron Decay	y	y	y	y	y	y	y	y	n
Cosmic Rays	n	n	n	y	n	y	n	n	n
Neutron Pulse	y	y	n	y	y	n	n	n	y
n-γ	y	y	n	y	y	n	n	n	y
Scattered e-p	y	y	y	y	y	y	y	y	y
Residual gas	n	n	y	y	n	y	y	y	y
HV discharge	n	n	n	y	n	y	y	y	y
Penning Ionization	y	y	n	y	n	y	y	y	y

5.9 Spectrometer Analyzing Power

In principle, the proton asymmetry can be measured with a single detector. The symmetric geometry proposed for PANDA has several significant advantages. First the coincidence rates are increased by an order of magnitude by counting all beta-proton coincidences (the beta and proton are highly anit-correlated due to kinematics), and of course a factor of two is gained by counting protons going in both directions. The symmetry of the PANDA spectrometer allows us, in essence, to simultaneously do two

nominally identical experiments; however this assumes that the analyzing power for the left and right sides are identical. In practice we do two separate experiments, each described by equation 25. Thus we would have $\mathcal{A}_L$ and $\mathcal{A}_R$. The spectrometer analyzing power must therefore consider both $\mathcal{A}_L + \mathcal{A}_R$ and $\mathcal{A}_L - \mathcal{A}_R$. Accurately determining these at the 10^{-3} level is the most significant challenge for PANDA.

The analyzing power can differ from unity for a number of reasons including proton backscattering, electron backscattering that has a left-right asymmetry and a magnetic field profile that has a left-right asymmetry. Flipping the neutron spin with the RF flipper and with the ^{3}He polarization reversal will mitigate such effects to the extent that they are constant or slowly varying. (Patch effects are an example of a cause of a time varying effect.) Though electrons detected in either detector satisfy the coincidence requirement, a false asymmetry could arise due to the combination of the beta-asymmetry and electron backscattering or other position dependent electron detection efficiency.

5.9.1 Magnetic Mirror Effects

Magnetic mirror effects arise due to imperfections in the spectrometer magnetic fields. Figure 23 shows an event in which a beta "bounces" from a rise in the magnetic field. Such events can affect the spectrometer analyzing power because they will in general be different for the two sides of the spectrometer. With the magnetic field maximum at the center of the spectrometer (see Figure 21),

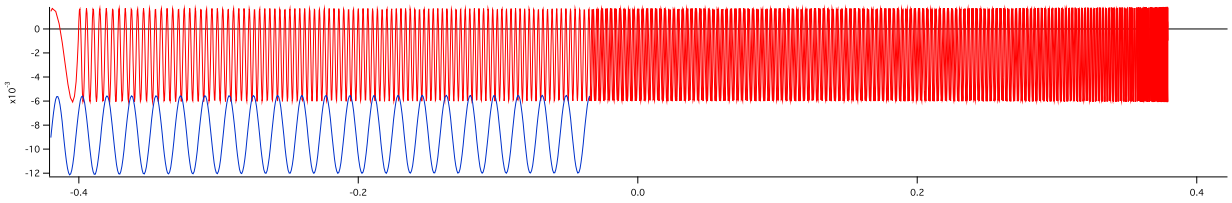

Figure 23: A simulated event demonstrating the potential for a proton to "bounce" from an imperfection in the magnetic field. In this event the proton (red) and electron (blue) are emitted in opposite directions from a vertex at (-3.4,-0.6) cm. The proton emission angle is 65° with respect to the spectrometer axis. The proton encounters a rise in the axial magnetic field at x = 38 cm and is reflected back toward the left. At x=-40 cm, the electric field accelerates the proton to a final energy of 24 keV, and it is detected in the Left SBD.

only imperfections will be a problem.

5.9.2 Residual Gas Scattering

The residual gas for vacuums below 10^{-8} torr will be mostly H_2. Proton scattering from H_2 at energies below 1 keV is mostly small angle scattering form atomic electrons and probability of protons scattering before they hit the detector at 10^{-8}torr is about 1.5% per meter, but the proton orbits cover up to several meters. Rutherford scattering (backscattering) will affect the spectrometer analyzing power. This must be included in the full scale modeling of the experiment. An asymmetric analyzing power would arise if the residual gas has a gradient due to any kind of leak and thermal differences. This should be small.

5.9.3 Penning Ions

Negative charge trapping due to positive potential well in the fiducial volume will change the electrostatic potential. A simple calculation shows that a negative ion density of order 10^{10} ion/cm^3 will produce a few volts of potential. The density of the residual gas atoms at 10^{-8} torr is 3×10^{11} molecules/cm^3. It is unlikely that the negative charge density will be a large fraction of the residual gas density.

5.9.4 Electric field patch effects

It is well known that the orientation dependent work function of individual metallic grains ("patch" effect) can give rise to local electric potential variations of order several 100 mV very close to a metallic surface (In this context, "very close" means on the order of the dimensions of an individual grain). The hope is that the patch effect averages to zero when the distance to the surface becomes large, but experience from the aSPECT experiment shows that this is not necessarily the case for technical surfaces[46]. The reasons are not yet understood, impurities in or on the surface coating might be responsible of their finding, which is a variation of the work function 100 mV over a distance of 5 cm. In addition metallic surfaces have charged patches due to radiation. The effect can be as big as several Volts, though at radiation levels which are many orders of magnitude higher than in PANDA.

We can minimize the effect by considering different surface materials and treatments. We will coat the inside of the electrode, at least in the vicinity of the decay region, with evaporated gold, colloidal gold, colloidal carbon or similar material which has been shown to significantly reduce the work function inhomogeneities. Furthermore, we can test at the neutron beam if the radiation level there makes a difference. And finally, as we will not be able to measure inhomogeneities directly if their amplitude is below a meV, we will use the effect that protons that can be reflected by such small electric potentials arrive at the very end of the time of flight spectrum of the protons, and can thus be identified and removed, if necessary.

A proton source inserted into the center of the decay volume will be used if a practical design can be developed. We are working to engineer our proton source, developed for silicon detector studies, as a probe that can be inserted into the region of the spectrometer fiducial volume for studies of proton focusing.

5.9.5 Charge Trapping and Penning Ionization

Another aspect of the problem of particle trapping is trapped particles cause a time-dependent background as they leak out of the trap. The decay volume and the surrounding area form a deep penning trap for electrons with energy below 24 keV (nominally). This can cause a fluctuating background and, in the worst case, high voltages breakdowns and discharges which are a danger for the detector. The filling time constant due to electrons from neutron decay depends on the residual gas density. Experience from other experiments (i.e. the NIST lifetime measurement [8]) shows that typically a vacuum below 10^{-8} mbar is required. Strategies to remove these Penning trapped ions include wire grids around the decay volume but may cause systematic uncertainties. If the filling time constant is slow enough, the trap could be carefully emptied when necessary by slowly ramping down the high voltage.

A magnetic field line which connects two negative HV electrodes at a potential minimum with a depth in the order of 1 kV can easily cause penning discharges because the electrodes give rise to t Penning discharge, which starts with a positive rest gas ion. The discharge propagates toward the

electron and can produce several secondaries, which could be trapped if they collide with a residual gas atom or due to non-adiabatic processes which prevent them from being reabsorbed at one of the cathodes. These in turn, they ionize residual gas atoms. Proper design of the electrodes can avoids these problems.

5.9.6 Collimation and edge effects

The decay volume is defined by the collimated neutron beam and by collimators along the spectrometer axis. Radial collimation of the beta and proton orbits is dependent on the transverse momentum and thus affects the acceptance. If the neutron beam profile is homogeneous there is no first order false effected associated with the collimation, but for a neutron beam that is inhomogeneous along the x direction, false effects can arise. The constraints will be studied by Monte Carlo and measured with position sensitive neutron monitors or a neutron camera. If we omit the collimation diaphragms, the SBD would act as effective diaphragm. In this case, we may increase backgrounds and backscattering. The best configuration of spectrometer collimators will be studied in the detailed simulations.

5.9.7 SBD Efficiency

SBD efficiency in principle is cancelled in the spin-flip asymmetry of equation 25 as long as there is not coupling of the spin flipper with the SBD DA; however the two sides of the spectrometer will, in general measure different ranges of beta and proton energies, and thus different corrections will need to be applied. The best approach to measuring these differences is to use unpolarized runs, which will be practical with a ^{3}He spin-filter polarizer.

5.9.8 Scattering and backscattering

Scattering and backscattering from elements of the spectrometer, i.e. the collimators and the SBDs will be carefully modeled in the process of developing the final design. Proton backscattering from the SBDs at 24 keV is a small effect, less than 0.3% and a Left-Right asymmetry of 30% would be necessary to affect the results at the 10^{-3} level. Electron backscattering, however, is notoriously large, up to 20%. Any asymmetry in the electron backscattering will couple to the proton detection efficiency leading to a left-right asymmetry, thus it will be essential to ensure that electron backscattering is understood at the percent level. This requirement will be further quantified by the detailed modeling and simulations.

5.9.9 Electronic noise and crosstalk

Electronic noise and cross talk can introduce a false asymmetry. For example, the RF spin flipper could couple into the noise in the SBD electronics and effect a change of beta and/or proton detection efficiency that is correlated with the neutron spin. This can be measured by using x-ray sources with the neutron beam off but the spin flipper running. The separate spin-flip that would be provided by a ^{3}He spin-filter polarizer would change the sign of and effectively cancel such effects to a high degree.

5.9.10 Analyzing Power Summary

Table 4 summarizes the contributions to the uncertainty and asymmetry of the spectrometer analyzing power. In general, we expect each of these to be understood to better than 10^{-3} by design based on extensive simulations and by direct measurement. Unpolarized runs are the best way to measure

the spectrometer analyzing power. These would be practical with the development and ultimately the installation of the ^{3}He spin-filter polarizer.

Table 4: Sources of error for the spectrometer analyzing power.

Source
Magnetic Mirror Effects
Patch Effects
Proton Backscattering
Electron Backscattering
Proton Residual Gas Scattering
Electron Residual Gas Scattering
Scattering
SBD Efficiency
Noise and crosstalk

5.10 Spectrometer Analyzing Power Studies - Simulations

A full Monte Carlo simulation of the spectometer is in progress. This includes accurate tracking of events, scattering and backscattering from all components of the spectrometer, in particular collimators and detectors, detector simulation with noise and finite resolution. These are based on the event generator developed at Michigan for the emiT analysis with recoil order and radiative corrections added. The events are tracked by a 4th order Runge-Kutta routine based on that developed for the NIST Radiative Neutron Decay (RDK) experiment. Electric field simulation is also based on the code developed for the RDK experiment. Residual gas scattering, collimators, backscattering and SBD response will be added to in order to establish a simulation package for the final design. Modules and data from GEANT4 will be incorporated as necessary and useful.

5.11 Energy Calibrations and Kinematics

Extracting physics from A_p and from C requires knowing the efficiency for detecting beta-proton coincidences as a function of the energy of both. For electron energy spectroscopy, SBDs will be calibrated in place with standard x-ray sources. For the cold bore spectrometer, a load-lock port at each end will be required to place the detector packages and calibration sources, etc. It will be useful to access the decay region through a separate load locked port in the spectrometer magnet gap. Proton energy dependence will be studied with the retarding potential, V_0 shown in Figure 6.

5.12 Initial neutron velocity

The initial velocity of the neutron velocity before decay adds vectorially to the beta and proton velocities. This is included in the simulations.

5.13 False Asymmetries

False asymmetries arise from any neutron spin-dependent effects are not perfectly cancelled by the symmetry of the spectrometer backgrounds, efficiencies and analyzing power, i.e the two sides of the spectrometer see different backgrounds and/or have different efficiencies. Thus they are all second-order, that is they are quantitatively determined by the product of two imperfections that we strive to make small to begin with. In the design and experimental approach described here, the uncertainties on each of these effects should be well below 1% and the product well below 10^{-3}.

5.14 Error Summary

Table 5 summarizes anticipated sources of error and the main strategy for each that will contribute to an overall error on the proton asymmetry below 10^{-3}.

Table 5: Sources of Error for PANDA@SNS

Error	Section	
Statistical Error	5.15	6 live days
Polarimetry and spin flip efficiency	5.1	time-of-flight dependence
Spectrometer Analyzing Power (Table 4)	5.9	calibration sources, unpolarized runs
Background Asymmetry	5.8	minimize backgrounds
Longitudinal Stern Gerlach	5.2	magnetic field mapping/simulation
Transverse Stern Gerlach	5.2	”
Spin Dependent Background Gammas	5.8	minimize backgrounds
Polarization Position Dependence	5.3	measure directly
Wavelength Resolution and Uncerainty	5.4	time-of-flight dependence
Time Dependent Polarization	5.5	measure directly
Time Dependent Backgrounds	5.8	minimize backgrounds
Time Dependent Analyzing Power	5.5	measure directly
Energy Calibration	5.11	calibration sources
Initial Neutron Velocity	5.12	simulations

5.15 Run Time Estimate

Our time estimate depends on the detector and DAQ performance and calculations of the FP13 flux presented in section 4.1. For high neutron polarization, spectrometer analyzing power, and spin flip efficicacy, the statistical error on C is approximately $\sigma_C \approx 1/\sqrt{N_p}$. From Figure 19, we see than for a 1.8 T field, a decay rate of about 35 s^{-1}, and we could expect an error of about 0.4% of C per live day with 0.1% precision reached in about six live days. Thus the experiment will not really be statistics limited, rather, in order to study systematic effects the asymmetry will be measured as a function of a number of parameters, *e.g.* neutron time of flight, proton energy, position, etc.

6 Upgrade path and improvements

The statistical power of this experiment makes promising the opportunities to consider upgrade the experiment. The asymmetry $kC \approx 0.25$ is relatively large, and the run time for a statistical error of 10^{-3} is 6 live days. This will allow extensive studies of systematic errors to achieve the overall goal of an error of 10^{-3} on C. Though it is unreasonable to project beyond what is in essence an order of magnitude improvement over the current state of the art in polarized neutron decay measurements, the potential for improved statistical power will motivate us to look to the next generation of PANDA.

The statistical power of PANDA is limited in part by the size of the SBDs. Less than 1/3 of the available neutron flux will be accepted by PANDA. A factor of 2-3 in rate can be gained with larger detectors such as those under development for abBA and Nab. Use of these detectors would lead to a change of the neutron collimation system and the collimation and baffles within the spectrometer. The position sensitivity of the abBA/Nab detector design would provide additional information that could be used to study effects such as scattering from the spectrometer baffles.

We are aggressively pursuing improvement of our understanding of polarized ^{3}He as a neutron spin filter. As we work this out, the opportunity to use ^{3}He will mitigate some of the potential compromises in understanding of systematics. With a ^{3}He spin filter, unpolarized runs to study backgrounds and spectrometer analyzing power will be possible, and the ^{3}He spin can be reversed, providing an additional spin flip to accompany the RF spin flipper.

A second generation PANDA@SNS experiment that is statistics limited will require further study and improvement of systematic errors discussed in this proposal. We believe that this proposal firmly establishes the feasibility of the first-gerenation measurement at the 10^{-3} level and will lead the way to a factor of 3 or more improvement in the second generation.

References

[1] C. Habeck, Experimental determination of the weak coupling constant ratio G_A/G_V in Neutron Decay, PhD Thesis, University of Sussex (1997).

[2] F. Glück, I. Joo, and J. Last, *Nucl. Phys. A* **593**, 125-150 (1995).

[3] F. Gluck *Phys. Lett.* **B376**, 25-28 (1996).

[4] M. Schumann, arXiv:0705.3769v1 [hep-ph].

[5] L. Lising, *et. al.*, *Phys. Rev.* **C62**, 055501 (2000).

[6] H. P. Mumm et al., *Rev. Sci. Inst* **12**, 5343 (2004).

[7] J. Byrne *et al.*, Phys. Rev. Lett **65**, 289-92, (1990).

[8] J.S. Nico *et al.*, Phys. Rev. **C71**, 055502 (2005).

[9] J. Byrne *et al.*, J.Phys.G, Nucl.Part.Phys. **28**, 1325-49, (2002).

[10] J.S. Nico *et al.*, Nature **444**, 1059 (2006).

[11] T.E. Chupp *et al.*, Nucl. Inst. Meth. **A 574**, 500 (2007).

[12] W-M Yao et al. (Particle Data Group), *J. Phys.* **G 33**, 1 (2006).

[13] A. Serebrov *et al.*, Phys. Lett. **B605**, 72 (2005).

[14] J.C. Hardy, I.S. Towner, *Phys. Rev.* **C71**, 055501 (2005)

[15] J. Hardy talk at INT: http://www.int.washington.edu/talks/WorkShops/int_07_36W/People/Hardy_J/Hardy2

[16] P. Herczyg, *Prog. Part. Nucl. Phys.* **46**, 413 (2001).

[17] G.J. Mattews, T. Kajino, T. Shima, Phys.Rev. **D71**, 021302(R) (2005).

[18] N. Severijns, M. Beck, I. Naviliat-Cuncic, *Rev. Mod. Phys.* **78**, 991 (2006).

[19] J.D. Jackson, S.B. Treiman, H.W. Wyld Jr. *Nucl. Phys.* **4**, 206 (1957).

[20] S. Ando, H. W. Fearing, V. Gudkov, K. Kubodera, F. Myhrer, S. Nakamura and T. Sato, Phys. Lett. **B 595**, 250 (2004).

[21] B.R. Holstein, Rev. Mod. Phys. **46**, 789 (1974); Rev. Mod. Phys. **48**, 673 (1976), Erratum.

[22] V. Gudkov, G. Greene, J. Calarco, Phys. Rev. **C 73**, 035501 (2006).

[23] V. Gudkov, *private communication.*

[24] S. Weinberg, Phys. Rev **115**, 481 (1959).

[25] G.L. Greene, private communication and P.R. Huffman *et al.Journal Research of NIST* **100**, 161 (2005).

[26] M. Kreuz, V. Nesvizhevsky, A. Petoukhov, T. Soldner, Nucl. Inst. Meth. **A 547**, 583 (2005).

[27] T. Soldner and A. Petoukov *private communication.*

[28] T.E. Chupp and K.P. Coulter, *Phys. Rev. Lett.* **55**, 1074 (1985).

[29] K.P. Coulter et al., *Nucl. Inst. and Meth.* **A270**, 90 (1988).

[30] T. Chupp, R. Holt, R. Milner, *Annual Reviews of Nuclear and Particle Science* **45**, 373 (1994).

[31] K.P. Coulter et al., *Nucl. Inst. and Meth. in Phys. Res.* **A24** 288, 463 (1989).

[32] G.S. Mitchell et al., *Nuc. Instr. Meth.* **A 521**, 468-479 (2004).

[33] P. Achenbach et al., *European Physics Journal* **A 25**, 177 (2005).

[34] Heil W, Dreyer J, Hofmann D, Humblot H, Lelievre-Berna E, Tasset F *Physica B* **268**, 328 (1999).

[35] T.E. Chupp and S.D. Swanson, *Advances in Atomic Molecular and Optical Physics* **43**, 42 (2000).

[36] E.J.R. van Beek , J.M. Wild , H.U. Kauczor, W. Schreiber ,J.P. Mugler , E.E. de Lange, *J. Mag. Res. Imaging* **20**, 540 (2004).

[37] L. Passel and R.I. Shirmer, *Phys. Rev.* **150**, 150 (1966).

[38] D.R. Rich, T.R. Gentile, T.B. Smith, A.K. Thompson, G.L. Jones, *Appl. Phys. Lett.* **80** , 2210 MAR (2002).

[39] E. Babcock *et al.*, Phys. Rev. Lett. 96 96, 083003 (2006).

[40] K.P. Coulter et al., *Nucl. Inst. and Methods* **A276**, 29 (1989).

[41] T.E. Chupp et al., *Phys. Rev.* **C 45**, 915-930 (1992).

[42] E. Babcock. B. Chann. I.A. Nelson, T.G. Walker , *Applied Optics* **44**, 3098 (2005).

[43] KH Andersen et al, Physica B 356, 103-108 (2005); E. Lelievre-Berna, Physica B 397, 162-167 (2007).

[44] W.H. Kraan, S.V. Grigoriev, M.T. Rekveldt, H. Fredrikze H, C.F. Vroege C.F.J. Plomp, *Nucl. Inst. Meth.* **A**, 334 (2003).

[45] M.J. Berger, S.M. Seltzer, Electron and Positron Energy Loss, WASHINGTON, NASA, 1964 131 P REFS PARTLY SUPERSEDED BY NASA-SP-3036, SEE N67-14099 (http://ntrs.nasa.gov/archive/nasa/casi.ntrs.nasa.gov/19650002905_1965002905.pdf).

[46] S. Baessler, *private communication.*

[47] F. Gluck *et al.* Eur. Phys. J. **A 23**, 135 (2005).

[48] J. Bonn *private communication*

[49] A. Pethoukov *et al. private communication* - to be published.

7 Facility Requirements

PANDA is a major undertaking for the FnPB. ORNL scientists are collaborators and will be essential in interfacing the collaboration to the experiment at FnPB. ORNL collaborator responsibilities will include the ^{3}He analyzer and possibly polarizer and the beam and cave. Engineering support during the design phase and technician support at the level of a full FTE for 6 months will be required to set up the experiment. Computer support will also be required at a level to be determined. Full support of all technical facilities (electrical, environmental, computing, and experiment control) will be required during set-up at data taking.

PANDA anticipates two three month runs at FnPB.

8 Schedule

PANDA requires 1) PRAC approval; 2) Funding; 3) Construction phase; 4) Data. The following schedule is optimistic; however with the funding in place procurement over the subsequent 1.5 years is consistent with the first run completed by the end of 2011. Based on the result from Run 1, we anticipate a second run in 2012.

PRAC approval: March 2008
Final Design complete: January 2009
Funding: March 2009
Supermirror complete: January 2010
Spin flipper complete: September 2009
Guide Field complete: December 2009
^{3}He spin filter (if possible): January 2010
Magnet complete: March 2010
Spectrometer Complete: September 2010
Assembly complete: December 2010
Commissioning: January 2011
Run 1 compete: December 2011

9 Manpower

The PANDA collaboration brings to the experiment significant expertise and experience in polarized neutron decay experiments, neutron polarization and polarimetery. The PANDA collaboration is largely distinct from several other collaborations working in fundamental neutron physics in the US. This is important, because it is essential to have the personnel resources to focus on the experiment and measurement. The community is working hard to bolster the number of collaborators working in the field, but we are, quite honestly, spread quite thinly. The following list of tasks and responsibilities has gaps, but also identifies experts who will apply their expertise to the essential pieces of the experiment. Our expectation is that approval of PANDA will lead to 1) collaborators focus on their roles in PANDA, 2) funding to support PANDA and collaborators working on PANDA, 3) new collaborators.

Repsonsibilities

Beam line, guides, collimation, shielding (ORNL)
Radiation issues (ORNL)
Upstream monitors
Supermirror polarizer (UVa/UKy/Michigan)
Spin transport fields (polarizer to experiment, experiment to analyzer) (ASU)
Spin flipper (Michigan/ORNL)
Spectrometer magnet (PANDA/Nab/abBA collaborations)
Magnetic shielding (two way) (ASU)
Spectrometer E fields (UVa/Michigan)
Experiment control
SBD detectors/proton gun (NIST/Michigan)
DAQ (NIST/Michigan)
^{3}He analyzer (polairzer) (ORNL/NIST/Michigan)
Analyzer detectors
Simulations (UVa/NIST/UMich/UKy)
Engineering/ Technical Coordination Beamline; Spectrometer
Scientific coordination
Analysis (graduate students)

10 Budget Estimates

Cost estimates of the components of PANDA are given below. The spectrometer and beam line estimates are assumed to be common to PANDA and abBA/Nab. In addition to the magnet and cryostat, some components of the spectrometer vacuum and HV system are common. The spin flipper coil and parts of the guide field may be the same for PANDA and abBA, but the spectrometer fields are different and thus the coupling of the guide field to the spectrometer field is different. The cave, shielding and beam dump are assumed to be common to all experiments in the beta-decay program.

	Item	Quantity	Unit cost	Cost
1.0	Beamline (from abBA)			
1.1	Design	2	7500	15000
1.2	Procurement	2	44000	88000
1.2.1	neutron guide - 2m	1	70000	70000
1.3	Cave/shielding	1	TBD	
1.4	Beam Dump	1	TBD	
	total beamline			173000
2.0	Spectrometer Magnet (from abBA/Nab)			
2.1	Design	1	7500	7500
2.2.1	magnet	1	950000	950000
2.2.1.1	power supplies	1	60000	60000
2.2.1.2	other cyogenics	1	20000	20000
2.3	HV insert	1	50000	50000
2.4	HV supplies	3	5000	15000
2.3	Installation	1	15000	15000
	total spectrometer			1117500
3.0	Guide Field			
3.1	Coils	6	4000	24000
3.2	Power Supplies	6	6500	39000
3.3	Control	2	4500	9000
	PANDA total			72000
4.0	Vasuum			
4.1	Vacuum Pumps	3	15000	45000
4.2	Vacuum Components	1	20000	20000
	Vacuum total			65000
5.0	SBD Detectors			
5.1	Detectos	6	6500	39000
	PANDA total			39000
7.0	PANDA DAQ			
7.1	Preamps	2	2400	4800
7.2	ADCs (Gage Cards)	2	14750	29500
7.3	Computers	2	2500	5000
7.4	Cables, connectors etc.	2	2500	5000
	total DAQ			44300
8.0	XSM Polarizer			
8.1	XSM supermirror	2	70000	140000
	total XSM			140000
9.0	3He Polarizer			
9.1	Oven	1	5000	5000
9.2	NMR	1	7200	7200
9.3	Heating system	1	8500	8500
9.4	Cells	5	TBD	
9.5	Laser	2	15000	30000
9.6	Optics	2	1600	3200
	total 3He spin filter			53900
10.0	3He Anzlyzer			
10.1	Cells	3	4000	12000
10.2	Oven	1	5000	5000
10.3	NMR	1	7200	7200
10.4	Heating system	1	8500	8500
10.5	Laser	1	15000	15000
10.6	Optics	1	1600	1600
	total analyzer			49300
11.0	Beam Monitors			
11.1	Monitors	3	15000	45000
11.2	DAQ Interface	3	2400	7200
	total beam monitors			52200
12.0	Spin Flipper (from abBA)			
12.1	Design	1	3000	3000
12.2	Procurement	1	10000	10000
12.3	flipper	1	10000	10000
12.4	RF source	1	10000	10000
12.5	solenoid	1	5000	5000
12.6	electronics	1	5000	5000
12.7	Installation testing	1	2000	2000
12.8	Commissioning	1	500	500
	total spin flipper			45500